

Arctic Ocean freshwater: How robust are model simulations?

A. Jahn,¹ Y. Aksenov,² B. A. de Cuevas,² L. de Steur,³ S. Häkkinen,⁴ E. Hansen,⁵ C. Herbaut,⁶ M.-N. Houssais,⁶ M. Karcher,⁷ F. Kauker,⁷ C. Lique,⁸ A. Nguyen,⁹ P. Pemberton,^{10,11} D. Worthen,^{4,12} and J. Zhang¹³

Received 19 January 2012; revised 21 May 2012; accepted 18 June 2012; published 10 August 2012.

[1] The Arctic freshwater (FW) has been the focus of many modeling studies, due to the potential impact of Arctic FW on the deep water formation in the North Atlantic. A comparison of the hindcasts from ten ocean-sea ice models shows that the simulation of the Arctic FW budget is quite different in the investigated models. While they agree on the general sink and source terms of the Arctic FW budget, the long-term means as well as the variability of the FW export vary among models. The best model-to-model agreement is found for the interannual and seasonal variability of the solid FW export and the solid FW storage, which also agree well with observations. For the interannual and seasonal variability of the liquid FW export, the agreement among models is better for the Canadian Arctic Archipelago (CAA) than for Fram Strait. The reason for this is that models are more consistent in simulating volume flux anomalies than salinity anomalies and volume-flux anomalies dominate the liquid FW export variability in the CAA but not in Fram Strait. The seasonal cycle of the liquid FW export generally shows a better agreement among models than the interannual variability, and compared to observations the models capture the seasonality of the liquid FW export rather well. In order to improve future simulations of the Arctic FW budget, the simulation of the salinity field needs to be improved, so that model results on the variability of the liquid FW export and storage become more robust.

Citation: Jahn, A., et al. (2012), Arctic Ocean freshwater: How robust are model simulations?, *J. Geophys. Res.*, 117, C00D16, doi:10.1029/2012JC007907.

1. Introduction

[2] The freshwater (FW) content of the Arctic Ocean and its export to the North Atlantic has been the focus of many

studies, due to the potential impact that a release of some of this FW to the North Atlantic could have on the deep water formation in the North Atlantic [e.g., *Aagaard et al.*, 1985; *Aagaard and Carmack*, 1989; *Weaver et al.*, 1993; *Häkkinen*, 1995; *Lohmann and Gerdes*, 1998; *Holland et al.*, 2001; *Rennermalm et al.*, 2006, 2007; *Arzel et al.*, 2008; *Rabe et al.*, 2011].

[3] In recent years, the number of hydrographic and current meter measurements in key Arctic straits and the Arctic Ocean itself has sharply increased, resulting in more accurate, mutually consistent observational estimates of the FW content [e.g., *Proshutinsky et al.*, 2009; *McPhee et al.*, 2009; *Rabe et al.*, 2010, 2011] and FW export [e.g., *Prinsenberg and Hamilton*, 2005; *Münchow et al.*, 2006; *Melling et al.*, 2008; *Münchow and Melling*, 2008; *de Steur et al.*, 2009; *Dodd et al.*, 2009; *Curry et al.*, 2011; *Tsubouchi et al.*, 2012]. However, these observational time series are still relatively short (around or under 10 years) and uncertainties of flux estimates from these measurements are too large to reconstruct interannual variability of FW in the Arctic with confidence [e.g., *Curry et al.*, 2011]. It is therefore no surprise that modeling is widely used to study the interannual-to-decadal variability of the Arctic FW export and storage. Most of these studies, however, use results from a single model, typically focusing on a specific physical phenomenon or process [e.g., *Zhang et al.*, 2003; *Karcher et al.*, 2005; *Köberle and*

¹National Center for Atmospheric Research, Boulder, Colorado, USA.

²National Oceanography Centre Southampton, Southampton, UK.

³NIOZ Royal Netherlands Institute for Sea Research, Den Burg, Netherlands.

⁴NASA Goddard Space Flight Center, Greenbelt, Maryland, USA.

⁵Norwegian Polar Institute, Tromsø, Norway.

⁶LOCEAN, UMR CNRS/UPMC/IRD/MNHN, Université Pierre et Marie Curie, Paris, France.

⁷Alfred Wegener Institute for Polar and Marine Research, Bremerhaven, Germany.

⁸Joint Institute for the study of the Atmosphere and the Ocean, University of Washington, Seattle, Washington, USA.

⁹Massachusetts Institute of Technology, Cambridge, Massachusetts, USA.

¹⁰Department of Meteorology, Stockholm University, Stockholm, Sweden.

¹¹Swedish Meteorological and Hydrological Institute, Oceanographic Research Unit, Norrköping, Sweden.

¹²Wyle Information Systems Group, McLean, Virginia, USA.

¹³Polar Science Center, Applied Physics Laboratory, College of Ocean and Fishery Sciences, University of Washington, Seattle, Washington, USA.

Corresponding author: A. Jahn, National Center for Atmospheric Research, Boulder, CO 80307, USA. (ajahn@ucar.edu)

Gerdes, 2007; Arzel et al., 2008; Condron et al., 2009; Lique et al., 2009; Jahn et al., 2010a, 2010b; Houssais and Herbaut, 2011]. This makes it difficult to assess how well a model represents real physical mechanisms and to what extent the results are model dependent. Model inter-comparisons are a useful method to evaluate the model dependence of results, and past Arctic model intercomparison studies have led to improvements in the models, after diagnosing biases [e.g., *Holloway et al., 2007; Karcher et al., 2007*]. For the Arctic FW budget, intercomparison studies have so far focused on simulations from CMIP3 climate models [*Holland et al., 2007; Rawlins et al., 2010*], documenting areas where improvements are needed and showing consistent features of these simulations. An inter-comparison study of the Arctic FW budget simulated by forced ocean-ice models, however, has been missing so far, despite the increased use of hindcast simulations from forced ocean-ice models to study aspects of the Arctic FW and its variability. To fill this gap and to establish how robust forced ocean-ice model simulations of the Arctic FW are and where improvements are needed, we here investigate the Arctic FW budget and FW export variability as simulated by a wide range of forced ocean-ice models participating in the Arctic Ocean Model Intercomparison project (AOMIP) [*Proshutinsky et al., 2011*], comparing the model results to observational data where possible. In this study it will be shown that the overall sink and source terms of the FW budget, the seasonal cycle of the liquid FW export, and the interannual variability of the solid FW export are simulated consistently in most models, while the models show larger disagreement on the interannual variability of the liquid FW export, especially in Fram Strait, as well as on the seasonal cycle of the solid FW export in the Canadian Arctic Archipelago (CAA).

[4] The outline of this article is as follows: In sections 2–3, we give an overview of the participating models and the observations we used. In section 4 we compare and discuss the climatological average FW fluxes and content, followed by a comparison of the interannual variability of the FW fluxes and content in section 5 and of the seasonal cycle of the FW exports in section 6. Finally, a summary is presented in section 7 and the conclusions follow in section 8.

2. Models

[5] The model output compared here comes from the forced ocean-sea ice models used by several groups participating in AOMIP. This study compares existing model simulations, performed with uncoordinated model forcing, set-up, model physics, and length of the integrations. This makes it impossible to conduct sensitivity studies of the results, but it gives an overview of the range of results obtained from many of the models frequently used to study Arctic Ocean processes. This allows us to evaluate how robust the results from individual models are and where shortcomings are found that need to be addressed in the future; to further investigate the reasons for the model differences, coordinated follow-up studies with a sub-set of the models are needed. In these studies, the difference in the simulated FW fluxes resulting from, for example, the use of different atmospheric forcing, different runoff data sets, and different initial conditions could be investigated.

Furthermore, studies with the same model at different resolutions can give insights into the complex relationship between horizontal resolution and simulated fluxes [e.g., *Fieg et al., 2010; Gerdes et al., 2008*]. The models we investigate here range from regional coupled ocean-sea ice models to global ocean-sea ice models, with a wide range of horizontal resolutions. An overview of the different models and simulations is given in Table 1, supplemented by short model descriptions in the following, which also provide references to other articles for more details.

2.1. ECCO2

[6] ECCO2 is a high-resolution global ocean and sea ice data synthesis that covers the full ocean depth and permits eddies. The ECCO2 solution is obtained by fitting a high-resolution (18 km horizontal grid spacing, 50 vertical levels) global-ocean and sea-ice configuration of the Massachusetts Institute of Technology general circulation model (MITgcm) [*Marshall et al., 1997; Losch et al., 2010*] to the available ocean and sea ice data. For this study, a pan-Arctic regional domain is used, which has the same resolution as the global solution. The domain boundaries are at 55°N in both the Atlantic and Pacific sectors and coincide with grid cells in a global, cubed sphere configuration of the MITgcm [*Menemenlis et al., 2005*]. The ice model mechanics follow a viscous plastic rheology and the ice momentum equations are solved numerically using the line successive over relaxation (LSOR) solver of *Zhang and Hibler [1997]*. Ice thermodynamics use a zero heat capacity formulation and seven thickness categories, equally distributed between zero to twice the mean ice thickness in each grid cell. Ice dynamics use only two thickness categories: open water and sea ice. Brine rejection during sea ice formation is treated using a sub-grid parameterization of *Nguyen et al. [2009]*.

[7] The integration period is 1992–2008, and initial conditions for January 1992 are from the World Ocean Atlas 2005 (WOA05) for temperature and salinity [*Locarnini et al., 2006; Antonov et al., 2006*] and from the Polar Science Center simulations with PIOMAS for sea ice [*Schweiger et al., 2011*]. Boundary conditions are from the optimized global ECCO2 solution [*Menemenlis et al., 2005*]. Surface boundary conditions (downward shortwave, downward longwave, wind, surface air temperature, relative humidity) are from the Japanese 25-year Reanalysis (JRA-25) [*Onogi et al., 2007*]. Monthly river run-off is based on the Arctic Runoff Data Base (ARDB) as prepared by P. Winsor (personal communication, 2007). No restoring or data assimilation is used. A detailed description and assessment of the ECCO2 solution is given in *Nguyen et al. [2011]*.

2.2. LOCEAN

[8] The LOCEAN model is a regional version of the ORCA05 ice-ocean model based on NEMO version 1.9 [*Madec, 2008*] coupled to the LIM2 sea ice model. A total of 46 vertical levels and a partial step formulation to accommodate the bottom topography are used. Vertical grid spacing is finer near the surface (6 m) and increases with depth to 250 m at the bottom. Vertical mixing coefficients are deduced from a turbulent kinetic energy closure scheme. The sea-ice model is the Louvain-la-Neuve model (LIM2), which is a dynamic-thermodynamic model specifically designed for climate studies. A detailed description is given

Table 1. Characteristics of the Different Sea-Ice Ocean Models Used in the Comparison^a

Model ID	Ocean Code	Sea Ice Physics	Model Domain	Horizontal Resolution	Vertical Levels	CAA Passages	Runoff	SSS Restoring	Forcing	Spin-Up	Analysis Period
ECCO2	MIT-gcm	VP/2LI	Arctic / NS	18 km	50	3	ARDB	None	JRA-25	None	1992–2008
LOCEAN	NEMO 1.9	VP/2LI	Arctic / NA	20 km	46	2	R-ArcNet	30 days/6 m	ERA40	23 yrs	1958–2001
NAOSIM	MOM 2	VP/2LI	Arctic / NS	28 km	30	2	AOMIP	180 days/20 m	NCEP	50 yrs	1948–2008
OCCAM	OCCAM	EVP/2LI	Global	8 km	66	4	incl. in restoring	40 days/5 m	NCEP	None	1989–2006
ORCA025	NEMO 1.9	VP/2LI	Global	10 km	46	3	DT02	36 days/6 m	DFSS	None	1958–2004
PIOMAS	POP	VP/ITD	Arctic / NS	22 km	30	2	AOMIP	Included in restoring	NCEP	30 yrs	1948–2008
POM	POM	GV/2LI	Arctic / NA	51 km	26	2	BS02	None	NCEP	None	1948–2008
POP2-CICE4	POP2-CICE	EVP/ITD	Global	47 km	60	2	DT02	292 days/10 m	CORE-v2	180 yrs	1948–2007
RCO	RCO	EVP/ITD	Arctic / NS	28 km	59	2	AOMIP	None	ERA40 & ECMWF	ice: 10 yrs ocean: none	1958–2008
UVic ESCM	MOM2.2	EVP/2LI	Global	64 km	32	1	R-ArcNet	None	Coupled, wind forcing from NCEP	298 yrs	1948–2007

^aAll ocean models are coupled to a sea-ice model. For sea ice physics, a distinction is made between viscous-plastic (VP), generalized viscous (GV) and elastic-viscous-plastic (EVP) rheologies and between ice thickness distribution (ITD) and two-level (2LI) [Hibler, 1979] thermodynamics. For models with variable horizontal resolution, the resolution is an estimate for the Arctic Ocean. The model domains vary from global to Arctic/North Atlantic Ocean (Arctic/NA) and Arctic/Nordic Seas (Arctic/NS). “CAA passages” stands for the number of exits to the North Atlantic through the CAA. Arctic runoff is taken from the Arctic Runoff data base (ARDB, P. Winsor, personal communication, 2007), Arctic Net (R-ArcNet) from Lammers *et al.* [2001], based on Dai and Trenberth [2002] (DT02), according to Barron and Smedstad [2002] (BS02); but with an additional discharge of 700 km³/yr uniformly distributed along the Eurasian Arctic coast), or follows the AOMIP protocol (AOMIP), based on Prange [2003] and available at <http://www.who.edu/page.do?pid=30587>. Note that one model (UVic ESCM) is a sea ice-ocean model coupled to an EMB atmospheric model. The time scale for the sea surface salinity (SSS) restoring is provided together with the thickness of the ocean layer where it applies.

in Timmermann *et al.* [2005]. The domain encompasses the Arctic Ocean and the Atlantic Ocean from 30°S and is forced at its open boundaries by monthly climatology of a global ORCA05 simulation. The horizontal resolution roughly varies from 20 km in the Arctic to 50 km at the equator. The Arctic Ocean connects to the Baffin Bay by two channels running into Lancaster Sound and Smith Sound. The model is initialized from rest with version 3 of the Polar science center Hydrographic Climatology (PHC) global ocean climatology (PHC3.0 updated from Steele *et al.* [2001]). Except for the precipitation extracted from the Coordinated Ocean Research Experiments (CORE) data set, daily atmospheric fields are taken from the ERA40 reanalysis [Uppala *et al.*, 2005] with some regional corrections applied to the radiation flux over the North Atlantic and to the surface air temperature (SAT) over the Arctic (in this last case, the ERA40 SAT climatology is replaced by the International Arctic Buoy Programme (IABP) climatology [Rigor *et al.*, 2000]). The river runoff is prescribed from the R-ArcticNET monthly climatology (<http://www.R-ArcticNET.sr.unh.edu>), based on Lammers *et al.* [2001]. The salinity in the 6-m top layer is restored to climatology with a time scale of 30 days. The 44-years (1958–2001) of model integration are preceded by a 23-year spin-up (see Herbaut and Houssais [2009] for details).

2.3. NAOSIM

[9] NAOSIM (North Atlantic-Arctic Ocean-Sea Ice Model), is a regional, coupled sea ice-ocean model developed at the Alfred Wegener Institute for Polar and Marine Research [Köberle and Gerdes, 2003]. It is derived from the Geophysical Fluid Dynamics Laboratory modular ocean model MOM-2 [Pacanowski, 1995] and a dynamic-thermodynamic sea ice model with a viscous-plastic rheology [Hibler, 1979]. The version used here has 30 unevenly spaced levels in the vertical. The model domain includes the Arctic Ocean, the Nordic Seas and the Atlantic Ocean north of approximately 50°N, with a horizontal resolution of 1/4° or 28 km. In contrast to the set-up presented in Köberle and Gerdes [2003], an open Bering Strait is introduced for which a constant net volume inflow from the Pacific Ocean of 0.8 Sv (25,000 km³/yr; 1 Sv = 10⁶ m³/s) has been applied. At the southern boundary and in the Bering Strait, open boundary conditions have been implemented following Stevens [1991], thereby allowing the outflow of tracers and the radiation of waves. The initial hydrography in January 1948 is adapted from the PHC winter climatology [Steele *et al.*, 2001], while a yearly mean climatology is used as a reference for surface salinity restoring on a time scale of 180 days. Parameterization of river runoff is employed using negative salt fluxes proportional to seasonal climatologies of runoff for each of the major rivers which follows the AOMIP protocol (<http://www.who.edu/page.do?pid=30587>), which is based on Prange [2003]. The model is driven with daily atmospheric forcing for 1948–2008 from the National Centers for Environmental Prediction/National Center for Atmospheric Research (NCEP/NCAR) reanalysis [Kalnay *et al.*, 1996] and initial conditions were taken from a 50 year spin-up experiment driven by a climatological atmospheric forcing. More details on the model can be found in Karcher *et al.* [2011].

2.4. OCCAM

[10] The OCCAM (Ocean Circulation and Climate Advanced Model) model is a high-resolution finite-difference z-level global model developed at the National Oceanography Centre and described in detail in *Aksenov et al.* [2010a, 2010b]. The model grid is combined from two spherical grids with nominal horizontal resolution of 1/12 degree. This results in model horizontal resolution being nearly-uniform globally, of ca. 8 km. The fine model resolution allows explicit simulation of eddies in most of the world ocean; in the Arctic Ocean the model is eddy admitting due to the small Rossby radius, but eddies larger than 25 km in diameter are resolved. The vertical resolution of the model increases from 5 m at the surface to 5–40 m in the upper 400 m and to 40–200 m in the deeper ocean. Due to the high model resolution, all four channels in the CAA (Nares Strait, Cardigan Strait, Barrow Strait and Fury and Hecla Strait) which connect the Arctic Ocean to the Labrador Sea are opened without topography alterations. Bering Strait is represented by a channel connecting the Pacific and Arctic Oceans. Other model features include a free surface ocean model [*Killworth et al.*, 1991] and partial bottom cell topography [*Adcroft et al.*, 1997; *Pacanowski and Gnanadesikan*, 1998]; the latter is essential in representing shelf water dynamics and flow through the CAA [*Aksenov et al.*, 2010a, 2010b], as well as simulating the Arctic boundary current [*Aksenov et al.*, 2011]. The ocean model is coupled to a sea ice model which uses ice dynamics with elastic-viscous-plastic (EVP) rheology [*Hunke and Dukowicz*, 1997] and Semtner thermodynamics [*Semtner*, 1976] with additional parameterizations for the snow ice formation, improved lateral sea ice melting, and partial freeze up of ocean cells to improve the simulation of young ice formation. The model sea surface salinity is relaxed to the monthly mean climatological values from WOA2005 [*Antonov et al.*, 2006] on a timescale equivalent to 40 days. This salinity relaxation also accounts for the runoff, so no runoff is prescribed separately. In the present analysis the simulations were initialized from rest, using temperature and salinity fields from WOA2005 [*Antonov et al.*, 2006; *Locarnini et al.*, 2006] together with sea ice and snow fields from *Romanov* [2004]. The model was integrated for 1985–2006, forced with 6-hourly wind, near surface air temperature and atmospheric pressure fields together with monthly cloudiness and humidity from the NCEP/NCAR reanalysis. The first 4 years of the integrations are used as model spin-up, so that the analysis is only done for 1989–2006.

2.5. ORCA025

[11] The ORCA025 coupled ocean/sea-ice model uses the same ORCA-LIM2 ice-ocean code based on the NEMO framework version 1.9 [*Madec*, 2008] as the LOCEAN model described earlier, with the same vertical resolution. However, in contrast to the LOCEAN model the ORCA025 is a global model that uses a two times higher horizontal resolution. Furthermore, the forcing is different between the LOCEAN and ORCA025 models and there is no spin-up for the ORCA025. The configuration of the ORCA025 that is used here was developed in the DRAKKAR project [*Barnier et al.*, 2007] and an overall description of the model and its numerical details are given in *Barnier et al.* [2006]. The

model uses a global tripolar grid with 1442×1021 grid points and 46 vertical levels. Vertical grid spacing is finer near the surface (6 m) and increases with depth to 250 m at the bottom. The partial step topography [*Adcroft et al.*, 1997; *Pacanowski and Gnanadesikan*, 1998] used in the model permits representation of small topographic slopes near the Arctic shelves, facilitating more realistic along-shelf flow [e.g., *Barnier et al.*, 2006; *Penduff et al.*, 2007]. Horizontal resolution is 0.25° , which translates to about 28 km at the equator, 14 km at 60°N , 10 km in the Arctic Ocean and 3–10 km in the CAA. The simulation runs from 1958 to 2004 with no spin-up. Initialization is done using PHC data. The forcing data set DFS3 is a blend of monthly precipitation, daily downward shortwave and longwave radiation from the CORE forcing data set [*Large and Yeager*, 2004] and 6-hourly 10 m wind, 2 m air humidity and 2 m air temperature from ERA40 reanalysis [*Brodeau et al.*, 2010]. River runoff rates are prescribed using the *Dai and Trenberth* [2002] climatological data set, which, on average, gives a 50% larger run-off compared to the R-ArcticNET values used in the LOCEAN model. To avoid an excessive model drift, we add a relaxation of sea surface salinity to the PHC climatology. The coefficient (0.167 m/day) amounts to a decay time of 36 days for 6 m of water depth; under the ice cover restoring is five times stronger (while it is kept uniform in the LOCEAN model). Details of the simulation and an assessment of the simulated FW budget can be found in *Lique et al.* [2009, 2010].

2.6. PIOMAS

[12] The PIOMAS model is the coupled pan-arctic ice-ocean modeling and assimilation system developed at the University of Washington [*Zhang and Rothrock*, 2003]. The sea ice model is the multicategory thickness and enthalpy distribution (TED) sea ice model [*Zhang and Rothrock*, 2001; *Hibler*, 1980]. The ice model mechanics follow a teardrop viscous plastic rheology [*Zhang and Rothrock*, 2005] and the ice momentum equations are solved numerically using the line successive relaxation solver of *Zhang and Hibler* [1997]. The ocean model is based on the Parallel Ocean Program (POP) developed at Los Alamos National Laboratory [*Smith et al.*, 1992]. The model domain of PIOMAS covers the northern hemisphere north of 49°N . The model is one-way nested to a global ice-ocean model [*Zhang and Rothrock*, 2003] with open boundary conditions along 49°N . The PIOMAS finite-difference grid is based on a generalized orthogonal curvilinear coordinate system with the “North Pole” of the model grid placed in Greenland. The model has a mean horizontal resolution of about 22 km for the Arctic, Barents, and GIN (Greenland-Iceland-Norwegian) seas, and Baffin Bay. The POP ocean model has 30 vertical levels of varying thicknesses to resolve surface layers and bottom topography. The upper six levels are 5 m thick. PIOMAS is driven by daily NCEP/NCAR reanalysis atmospheric forcing, and results are shown for 1948–2008. Model forcing also includes river runoff, following the AOMIP protocol [*Prange*, 2003]. The model was spun-up for 30-years, forced repeatedly by 1948 NCEP/NCAR reanalysis forcing, with initial conditions of zero ice and ocean velocity, 2 m ice thickness and ocean temperature and

salinity from Levitus 1982 [Levitus, 1982]. No data assimilation or restoring is performed for this study.

2.7. POM

[13] The POM model is a regional ocean-sea ice model with $0.35^\circ \times 0.45^\circ$ horizontal resolution, which corresponds to an average horizontal resolution of 51 km in the Arctic Ocean. The ocean model is hydrostatic and Boussinesq and the version used here uses a z-level coordinate system, with 26 vertical levels. The sea-ice model is a dynamic-thermodynamic ice model, which uses a generalized viscous rheology [Häkkinen and Mellor, 1992]. It is forced with monthly data from the NCEP/NCAR reanalysis for 1948–2008. Precipitation, evaporation, and runoff are climatological throughout the simulation and are added to the ocean model via virtual salt fluxes. The runoff climatology is taken from Barron and Smedstad [2002], but with an additional discharge of $700 \text{ km}^3/\text{yr}$ uniformly distributed along the Eurasian Arctic coast. No salinity-restoring is used. More details on the model can be found in Häkkinen and Proshutinsky [2004].

2.8. POP2-CICE4

[14] The POP2-CICE4 simulation is an ocean-ice hindcast for 1948–2007, using the ocean and sea ice components of the Community Climate System Model version 4 (CCSM4 [Gent et al., 2011]). The ocean model of the CCSM4 is based on the Parallel Ocean Program version 2 (POP2) [Smith et al., 2010] and the sea-ice model of the CCSM4 is the Los Alamos Sea Ice Model (CICE) version 4, also known as the Community Ice Code [Hunke and Lipscomb, 2008]. The model was run globally at a nominal resolution of 1° , with a rotated orthogonal grid. The average horizontal resolution in the Arctic Ocean is 47 km. The ocean model has 60 vertical levels (ranging from 10 m thickness at the surface to 250 m at depth), and includes near-surface eddy flux parameterization, an abyssal tidally driven mixing parameterization, a deep overflow parameterization, a sub-mesoscale mixing scheme, and vertically-varying thickness and isopycnal diffusivity coefficients (see Danabasoglu et al. [2012] for more details on the model). The sea-ice model is a dynamic-thermodynamic model that includes a sub-grid-scale ice thickness distribution [Thorndike et al., 1975; Lipscomb, 2001], energy conserving thermodynamics [Maykut and Untersteiner, 1971; Bitz and Lipscomb, 1999], and EVP dynamics [Hunke and Dukowicz, 1997].

[15] The simulation used here is part of the CORE-II suite of simulations (archived on the earth System Grid under the name g.b29.01) and is the NCAR contribution to the WGMOD CORE II protocol (www.clivar.org/organization/wgomd/resources/core/core-ii). It was forced by interannual fields from the CORE v2 IAF data [Large and Yeager, 2009] and monthly climatological river runoff based on Dai and Trenberth [2002]. Furthermore, a weak salinity restoring ($292 \text{ days}/10 \text{ m}$) flux was applied globally after subtraction of the global mean. The simulation was started from Levitus temperature and salinity [Levitus, 1982] and run for four cycles of the CORE-II forcing for 1948–2007, with the output from the last forcing cycle being used here.

2.9. RCO

[16] The Rossby Centre Ocean model (RCO) is a regional coupled sea-ice ocean model, here applied to the Arctic Ocean. The model domain covers the central Arctic Ocean including the Bering Sea and the North Atlantic roughly to 50°N . The horizontal resolution is $1/4^\circ$ or approximately 28 km in a rotated coordinate system centered over the North Pole. 59 vertical levels with layer thicknesses between 3 m at the surface and 200 m at the bottom are used, where the surface layer is allowed to undulate freely. In the North Atlantic Ocean an open lateral boundary is applied for both temperature and salinity fields using climatological monthly mean data of the PHC data set [Steele et al., 2001]. Along the Aleutian islands chain the boundary is closed, but to get a reasonable inflow through Bering Strait a volume flux is implemented as a river centered on the Aleutian arc with the flux spread out over several nearby grid points. The total volume flux applied is a climatological monthly mean value based on Woodgate et al. [2005].

[17] Surface boundary conditions (2 meter air temperature, 2 meter specific humidity, 10 meter wind speed, sea level pressure, precipitation and total cloudiness) are from the ERA-40 reanalysis project [Uppala et al., 2005] for the period 1958–2002 and ECMWF analysis products for the remaining period until the end of 2008. River run-off is provided by climatological monthly mean volume fluxes of 19 major rivers discharging into the Arctic Ocean and Nordic Seas, following the AOMIP protocol [Prange, 2003]. The total integration period is 1958–2008 where initial values of temperature and salinity are taken from PHC. The initial ice thickness distribution is taken from the end state of a previous simulation over 10 years whereas ocean currents and ice velocities are started from rest. No surface restoring is applied in this simulation. The sea-ice model is a multi-category thermodynamic-dynamic model that resolves the thickness distribution with 7 different ice classes [Mårtensson et al., 2012]. For further details of the RCO model, see Mårtensson et al. [2012], Meier et al. [2003], and Döscher et al. [2010].

2.10. UVic ESCM

[18] The UVic ESCM (version 2.8) is a global ocean-sea ice model coupled to an energy-moisture balance model (EMBM) for the atmosphere, developed at the University of Victoria [Weaver et al., 2001]. Energy and salt are conserved to machine precision, and no salinity or temperature restoring is used. The ocean component of the UVic ESCM is the Geophysical Fluid Dynamics Laboratory Modular Ocean Model (MOM), version 2.2 (see Pacanowski [1995] for details). The sea-ice model uses a zero-layer thermodynamic scheme with two categories (sea ice and open water). The dynamics are based on the EVP sea-ice model of Hunke and Dukowicz [1997]. The atmospheric component of the UVic ESCM is an EMBM that is loosely based on the model of Fanning and Weaver [1996]. It is forced by prescribed NCEP wind forcing [Kalnay et al., 1996], and heat and moisture are transported by advection. Runoff is prescribed from R-Arctic Net [Lammers et al., 2001]. The simulation used here is for 1948–2007 and has a horizontal resolution of 1.8° zonally and 0.9° meridionally, which corresponds to

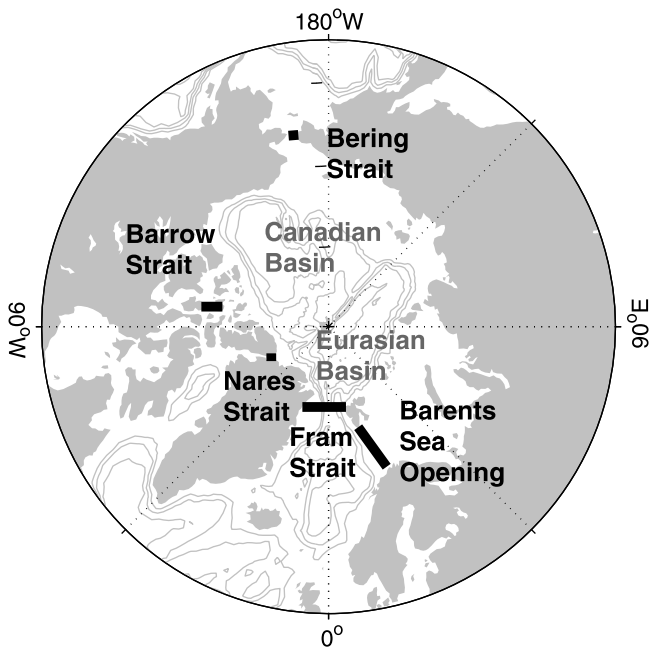


Figure 1. Map of the Arctic Ocean bathymetry (in grey contours, with contours every 1000 m, from 5000 m depth to 1000 m depth), the names of the deep basins as used in the text (in grey letters), and the location and names of the straits mentioned in the text (black letters).

an average resolution of 64 km in the Arctic Ocean. Note that there is an artificial island at the pole, because the grid has not been rotated. It has 32 unequally spaced vertical levels in the ocean (ranging from a thickness of 50 m at the surface to 298 m at the bottom). Details of the model, the simulation, and the simulated Arctic FW budget can be found in *Jahn et al.* [2010a].

3. Observations

[19] We compare the simulated FW fluxes with the FW budget compiled by *Serreze et al.* [2006], and also use the ice transport estimate through Bering Strait and the Barents Sea Opening from *Woodgate et al.* [2005] and *Kwok et al.* [2005], respectively. As the FW fluxes in *Serreze et al.* [2006] and many other papers are calculated relative to 34.8, the mean Arctic salinity according to *Aagaard and Carmack* [1989], we will also use 34.8 as reference salinity for our model intercomparison, to allow a comparison with published data. A map of the Arctic Ocean with the names of the straits and deep basins that are used in the text, as well as with the bathymetry of the Arctic Ocean, is shown in Figure 1.

[20] To assess the simulation of the liquid FW export through Fram Strait, we use the 10-year time series of mooring-derived FW fluxes in the East Greenland Current (EGC) between $6^{\circ}30'W$ and $0^{\circ}W$, at $78.83^{\circ}N$ [*de Steur et al.* 2009], but now calculated with a reference salinity of 34.8. For the seasonal cycle of the FW flux in Fram Strait, we compare the models with a new estimate of the mooring-derived seasonal cycle of the liquid FW flux for the EGC, which is based on a new method of dealing with the data gaps in the time series (*L. de Steur et al.*, manuscript in

preparation, 2012) relative to the estimate shown earlier in *de Steur et al.* [2009]. These gaps in the time series are related to instrument failure, lost instruments in the top of the mooring, or even completely lost moorings. The main difference in the analysis is the fact that gaps in the time series (due to missing velocity data) are reconstructed by regression of the time series on to data of the nearest instrument that has the highest correlation to the time series of the missing instrument in other years. Therefore the temporal variability of the total velocity field is resolved better. In addition, we calculate a range of possible upper-ocean salinities between the uppermost instruments at approximately 50 m depth and the surface since this is where the largest gradients in S may occur. This range is based on using different weights for the upper-ocean stratification obtained from summer hydrographic data (by 0%, 70%, 90% and 100%) relative to the salinity of the moored instruments. 0% implies no vertical stratification above 50 m but merely an extrapolation of the observed salinity from the moorings at 50 m, while 100% implies using a mean stratification from summer hydrography to extrapolate towards the surface. This provides an estimate of how sensitive the observational FW flux estimates are to extrapolating the salinity from the moorings to the surface, which is shown as error bars around the mean calculated seasonal cycle from the moorings in section 6. Furthermore, as the moorings were moved from $79^{\circ}N$ to $78.83^{\circ}N$ in 2002, which impacted the temporal variability of the data due to the complicated recirculation in the region, we only use the mooring data from 2002–2007 to compare with the seasonal cycle from the models.

[21] To compare the simulated solid FW export through Fram Strait to observational estimates we use the ice volume time series from *Vinje et al.* [1998], *Kwok and Rothrock* [1999], and *Kwok et al.* [2004]. For the fluxes through the CAA, we use published values from *Prinsenberg and Hamilton* [2005], *Kwok* [2005], *Münchow et al.* [2006], and *Münchow and Melling* [2008]. We also use updated data from Lancaster Sound to compare the seasonal cycle of the liquid FW export through this strait with the model simulations (*S. Prinsenberg*, personal communication, November 2011). This data contains 11 years of data for the liquid FW flux through Lancaster Sound. Note that these fluxes are estimates, and have a 20% uncertainty associated with them. We therefore use the standard deviation between the different years as an uncertainty estimate for the mean seasonal cycle. Furthermore, the period covered by the moorings is not the same as the longest period of overlap among the simulations (1992–2001), which complicates the comparison with the data. To assess the spatial patterns of FW storage, we use the salinity field from PHC data [*Steele et al.*, 2001] and ICESat-derived ice thickness data [*Kwok et al.*, 2009].

4. Climatological Averages

4.1. FW Budget

[22] The Arctic FW Budget simulated in the models shows significant differences, as can be seen in Table 2. For the analysis of the FW budget, all fluxes are averages over 1992–2001 and represent net fluxes through a strait (summing up all inflows and outflows over the full depth of a

Table 2. Arctic Ocean Freshwater (FW) Budget Relative to 34.8, Averaged Over 1992–2001, the Common Period Covered in All Simulations^a

	Observations	ECCO2	LOCEAN	NAOSIM	OCCAM	ORCA025	PIOMAS	POM	POP2/CICE4	RCO	UVIC-ESCM
River runoff	3200 ± 110	2532	2194	2456	2908*	3403	3916	3180	3334	3296	2767
Bering Strait liquid FW	2500 ± 300	2746	2830	1177	666	2976	1487	2102	1651	2109	1607
Net precipitation	2000 ± 200	2768	1710	1687	1557	2132	1211	2031	2075	1691	999
Bering Strait solid FW	100 ± 70	36	108	127	9	115	43	36	29	100	0
CAA liquid FW	−3200 ± 320	−3528	−5157	−548	−3091	−4677	−1904	−494	−3043	−2732	−2457
Fram Strait liquid FW	−2660 ± 528	−1389	−2703	−2831	−1408	−1989	−1439	−3222	−1504	−2054	−1120
Fram Strait solid FW	−2300 ± 340	−1682	−1934	−2675	−1893	−1761	−1704	−1559	−1654	−1629	−911
CAA solid FW	−160	−26	−127	−56	−8	−507	−17	−36	−236	−499	−108
BSO liquid FW	−90 ± 94	−337	−445	−426	−239	−269	−1136	−137	−752	2029	−954
BSO solid FW	−40	−247	−76	−215	−138	−202	−424	−22	−177	−112	−442
Liquid FW storage	74000 ± 7400	71811	89712	62867	58154	87013	73794	54961	78586	53432	86478
Solid FW storage	10000	13015	13005	21291	18579	16420	17291	12208	9495	15268	6474
Arctic Ocean area	10.0	10.2	8.9	10.1	11.1	12.0	9.7	9.9	10.0	9.3	9.6

^aAll observational values are taken from *Serreze et al.* [2006], except for the Bering Strait and BSO solid FW fluxes, which are based on *Woodgate and Aagaard* [2005] and *Kwok et al.* [2005], respectively. If available, error estimates for the observations are given as well. All FW fluxes are quoted in km³/year, and the FW storage is quoted in km³. They are annual mean net fluxes through a channel, combining negative and positive fluxes through a strait, where applicable. For the OCCAM model, the runoff term (denoted by an asterisk) is actually the restoring term, as no runoff is prescribed. All oceanic fluxes are calculated over the full depth of the water column at the boundaries. Positive values indicate FW sources, and negative values indicate FW sinks for the Arctic Ocean. The solid FW flux/storage includes FW from the snow on the ice as well as from the ice itself; however, the observational estimates only include the FW in the ice, which leads to a difference of about 10%. Note that due to an average over only 10 years and the use of salinity restoring in some models (see Table 1), the total of the FW fluxes in and out of the Arctic is not zero. Arctic Ocean area gives the area (in million km²) over which the liquid and solid FW storage is calculated in each model. For the location of the straits, see Figure 1.

strait, with negative fluxes representing a sink of FW for the Arctic Ocean). Despite the differences among the ten models, they all agree on the general view of the Arctic FW budget, with river runoff, net-precipitation, and Bering Strait inflow being the main sources of FW for the Arctic, and liquid and solid FW export through the Fram Strait and the CAA being the main sinks. The relative or absolute magnitude of all of these fluxes, however, do not agree across the investigated models, as discussed in the following.

[23] Comparing the sources of the FW budget from all ten models with each other and with the observations, we find that in all but one model (LOCEAN) the river runoff is the largest FW source for the Arctic. This is in agreement with observational estimates (taken from the compilation of *Serreze et al.* [2006]). Furthermore, in six models the simulated Bering Strait FW input is larger by at least 100 km³/yr than the net-precipitation (i.e., precipitation minus evaporation over the Arctic Ocean area), again in agreement with observational estimates. However, two models show the opposite and two more models show almost equal fluxes for these two FW sources (within ±100 km³/yr), due to the use of different reanalysis products for the precipitation and differences in the simulated flow through Bering Strait as well as in the evaporation. All but one model (UVic ESCM) also show a small addition of FW to the Arctic through the import of sea-ice through Bering Strait, which agrees with observations from *Woodgate and Aagaard* [2005]. The Barents Sea Opening is a net-source of FW in only one model (RCO), while the remaining nine models and the observational estimates show it as a net-sink of FW to the Arctic Ocean, primarily due to the import of water with salinities larger than the reference salinity of 34.8.

[24] All models agree that the largest solid FW export occurs through Fram Strait. This result is in agreement with

observations and is mainly a consequence of the narrow passages in the CAA that impede sea ice flow, limiting sea ice transports. For the liquid FW export, eight of the ten models show the largest net liquid FW export through the CAA, with less net liquid FW export through Fram Strait, as suggested by the FW budget from *Serreze et al.* [2006]. It is not immediately clear why the models disagree on the partitioning of the liquid FW export between the CAA and Fram Strait, as the two models that show a larger net liquid FW flux through Fram Strait than through the CAA are not the models with the highest or lowest resolution (NAOSIM, POM). Possible factors could be the cross-sectional areas of the CAA straits, which depend on the nominal resolution and on alterations of the model topography, as well as differences in the choices for the lateral boundary conditions (free slip or no slip), and differences in the simulated oceanic circulation in the Arctic. To really determine the role of these and other factors on the partitioning of the liquid FW export east and west of Greenland, a coordinated sensitivity study would be needed.

[25] Looking at the fluxes through the individual channels of the CAA, we find that eight out of the nine models with at least 2 open CAA channels show the largest FW export through Barrow Strait, with smaller fluxes through Nares Strait, and, if open, other smaller channels (see Table 3). In these models, the net liquid FW flux through Barrow Strait ranges from 56% to 86% of the total liquid FW export through the CAA and 14% to 44% through Nares Strait. The one model that has two channels but shows a larger liquid FW export through Nares Strait rather than Barrow Strait is the POP2-CICE4 models, which shows a larger FW flux through Nares Strait even though its cross sectional area is smaller than the cross sectional area of Barrow Strait (13 km² versus 36 km², respectively). These results highlight that not

Table 3. Net FW Flux Through the Channels of the CAA (km³/yr)^a

	ECCO2	LOCEAN	NAOSIM	OCCAM	ORCA025	PIOMAS	POM	POP2/CICE4	RCO	UVIC-ESCM	Observations
Barrow Strait liquid FW	-2288	-2881	-385	-1966	-3056	-1396	-812	-580	-2349	-2457	-1510 ^x
Barrow Strait solid FW	-26	-101	-13	-23	-198	-17	-36	-14	-282	-108	-76 ^x
Nares Strait liquid FW	-1240	-2276	-163	-677	-1747	-506	-356	-2463	-383	-	-788 ^o
Nares Strait solid FW	0	-27	-43	-21	-232	0	0	-222	-218	-	-119 ^s
Other opening liquid FW	0	-	-	-274	-574	-	-	-	-	-	-750*
Other opening solid FW	0	-	-	-4	0	-	-	-	-	-	unknown

^aThe maximum number of open CAA channels in some of the models is four. Observations are based on values reported in the literature, with values from *Prinsenberg and Hamilton* [2005] (denoted by a superscript x), *Münchow et al.* [2006] (denoted by a superscript o), and *Kwok* [2005] (denoted by a superscript s), calculated from the ice volume flux using an ice density of 910 kg/m³. Note that the estimate of the Nares Strait liquid FW flux (denoted by a superscript o) does not contain FW in the top 40 m, where a large part of the liquid FW export likely takes place, which means that this observational estimate is likely an underestimate of the actual liquid FW flux through Nares Strait (H. Melling, personal communication, December 2011). The Barrow Strait solid FW transport is based on the estimate of the export of solid FW through Lancaster Sound from *Prinsenberg and Hamilton* [2005], which includes solid FW grown within the CAA, whereas the Nares Strait solid FW estimate from *Kwok* [2005] is based on the inflow of ice from the Arctic into Nares Strait. The value for the liquid FW export through the “other” CAA channels (denoted by an asterisk) is based on personal communication with H. Melling (December 2011).

just resolution but also dynamical reasons can impact the flow through a strait, and that models may have reasonable net FW fluxes through a strait, but not necessary the right details of the flow.

4.2. FW Storage

[26] The total liquid FW storage averaged over the Arctic (Table 2) also varies among models, from 53,432 km³ to 89,712 km³. And while the area over which the Arctic FW storage is calculated varies among models (last row in Table 2), this does not seem to be the only factor leading to the differences. Looking at the distribution of the liquid FW storage (Figure 2a), we see clear differences among the models, both in the spatial pattern and in the magnitude of the FW column. Nevertheless, all models except the RCO show a clear maximum of the FW storage in the Beaufort Sea region for 1992–2001 (Figure 2a), as expected from the climatological PHC data [*Steele et al.*, 2001]. Note that we do not expect an exact match between the PHC data and the model simulated FW content for 1991–2002, as the PHC data are biased towards the 1970s and 1980s and recent observational data suggest significant changes in the shape and magnitude of the Beaufort Gyre on decadal timescales [*Proshutinsky et al.*, 2009; *Rabe et al.*, 2011]. We find that compared to the PHC data the models consistently show a shift of the FW content maximum towards the Canadian coast, in agreement with the observational results from *Proshutinsky et al.* [2009] for the 1990s. An exception is the ECCO2 model, which shows a liquid FW column similar to the PHC data. As ECCO2 lacks a spin-up and was started from prescribed conditions in 1992, the close agreement of the 1992–2001 average with the PHC data is likely due to the short time since initialization.

[27] For the solid FW storage, the models also show a range of FW storage averaged over the Arctic (Table 2), ranging from 6,474 km³ to 18,579 km³. This range mainly reflects differences in the simulated sea-ice thickness, with two models showing very thin sea-ice (UVic ESCM and

POP2-CICE4; see Figure 2b). Interestingly, the CORE II forced POP2-CICE4 model shows a much thinner sea-ice cover than in the fully-coupled simulation with the CCSM4 for the late 20th century [see *Jahn et al.*, 2012], in which the POP2-CICE4 is the ocean-ice component, using the same resolution and the same parameters. This shows that not only differences in the model physics or in the resolution but also the atmospheric forcing applied to the models, and the tuning of the models to this forcing, play a key role for the sea-ice simulation.

[28] In order to compare the simulated solid FW column with observations, we make use of the only currently freely available gridded data of sea-ice thickness, which are the sea-ice thickness data derived from ICESat by *Kwok et al.* [2009]. The ICESat-derived sea-ice thickness data are available for periods in winter (Feb–March) and fall (Oct–Nov) between 2003–2008. To compare the simulation results with this data, despite the different periods of the models (1992–2001) and the ICESat data (2003–2008), we average the ICESat data from winter and fall over 2003–2008 to arrive at an estimated “annual” mean ice thickness. In the models, an average of the February, March, October and November ice thickness provides a close match to the annual ice thickness (not shown), which gives this approach some merit; however, an actual annual average of the ICESat derived data would obviously be preferable. All models show thinner sea ice towards the Siberian coast and thicker sea ice towards the CAA (Figure 2b). Overall, most of the models (for 1992–2001) tend to overestimate the ice thickness when compared to the ICESat thickness field for 2003–2008, except the POP2-CICE4 and UVic ESCM models, which have clearly a too thin sea-ice cover. Over the last decade, however, the ice has thinned considerably [*Kwok et al.*, 2009], and if we compare the solid FW storage from 2004 among the nine models that have data for 2004 (all except LOCEAN; comparison not shown), we see a thinning in the simulated ice thicknesses. Furthermore, we also see some shift of thicker ice towards the Eurasian Basin in the

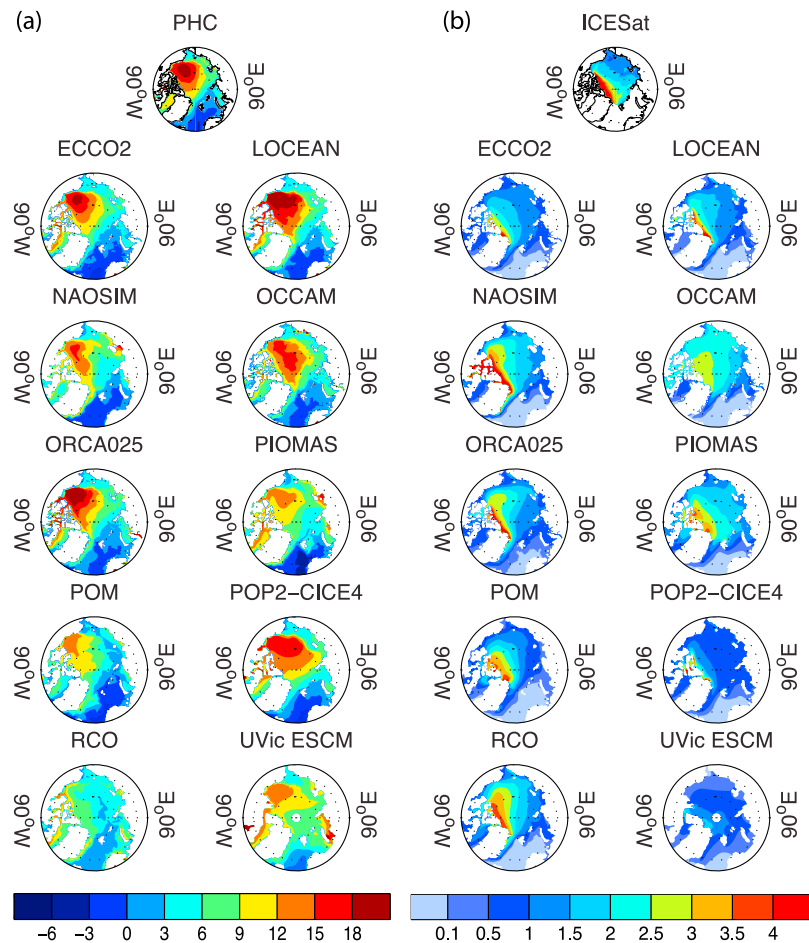


Figure 2. (a) Liquid and (b) solid FW storage in the Arctic (relative to 34.8 and for the top 250 m), shown as 10-year average (1992–2001) FW column (in m). The top row shows available observational estimates, from the PHC salinity climatology [Steele *et al.*, 2001] for the liquid FW column and from the ice-thickness data from ICESat [Kwok *et al.*, 2009] for the solid FW column. The solid FW column was calculated from the ICESat-derived ice thickness fields for spring and fall in 5 years (2003–2008), assuming a salinity of 4 in the sea-ice and an ice density of 917 g/m^3 . As only spring (February–March) and fall (October–November) data are available, these were averaged to obtain an approximate annual average (see text for details). White areas indicate the land mask for the individual models (and in the case of the ICESat data, also regions where no data are available).

simulations for 2004 that leads to a better match with the ICESat pattern than for the 1991–2002 period.

5. Interannual Variability

5.1. FW Export Variability

[29] In this section, we analyze the FW export variability. Due to the focus on the variability of the FW export, we focus on the outflowing FW only, rather than on the net fluxes as in section 4.1. Furthermore, in Fram Strait we limit the analysis to the top 250 m, which is where most of the FW export takes place.

5.1.1. Statistics

[30] In addition to differences in the mean of the FW export, as already described in section 4.1 and seen in Table 2, the statistics of the simulated liquid FW export also show differences among the models, as can be seen in Figure 3. Over the 10-year period from 1992–2001, the

standard deviation of the annual mean southward flux of liquid FW through Fram Strait between the surface and 250 m depth varies between $158 \text{ km}^3/\text{yr}$ (UVic-ESCM) and $622 \text{ km}^3/\text{yr}$ (POM). The variability over the full available simulation-length of each model is more difficult to compare, due to the large range of simulation lengths from 17 to 61 years. We note, however, that in all models the freshwater transport through Fram Strait shows a larger inter-annual standard deviation for their full simulation length compared to the 1992–2001 period. In some models (e.g., ECCO2, NAOSIM, and RCO) mean liquid FW export changes significantly when averaged for the full-length of the integrations and for 1992–2001 (Figure 3a). This suggests substantial interdecadal variability of the FW export from the Arctic, and together with a significant increase in the observed FW content in the Arctic during recent years [McPhee *et al.*, 2009; Proshutinsky *et al.*, 2009; Rabe *et al.*,

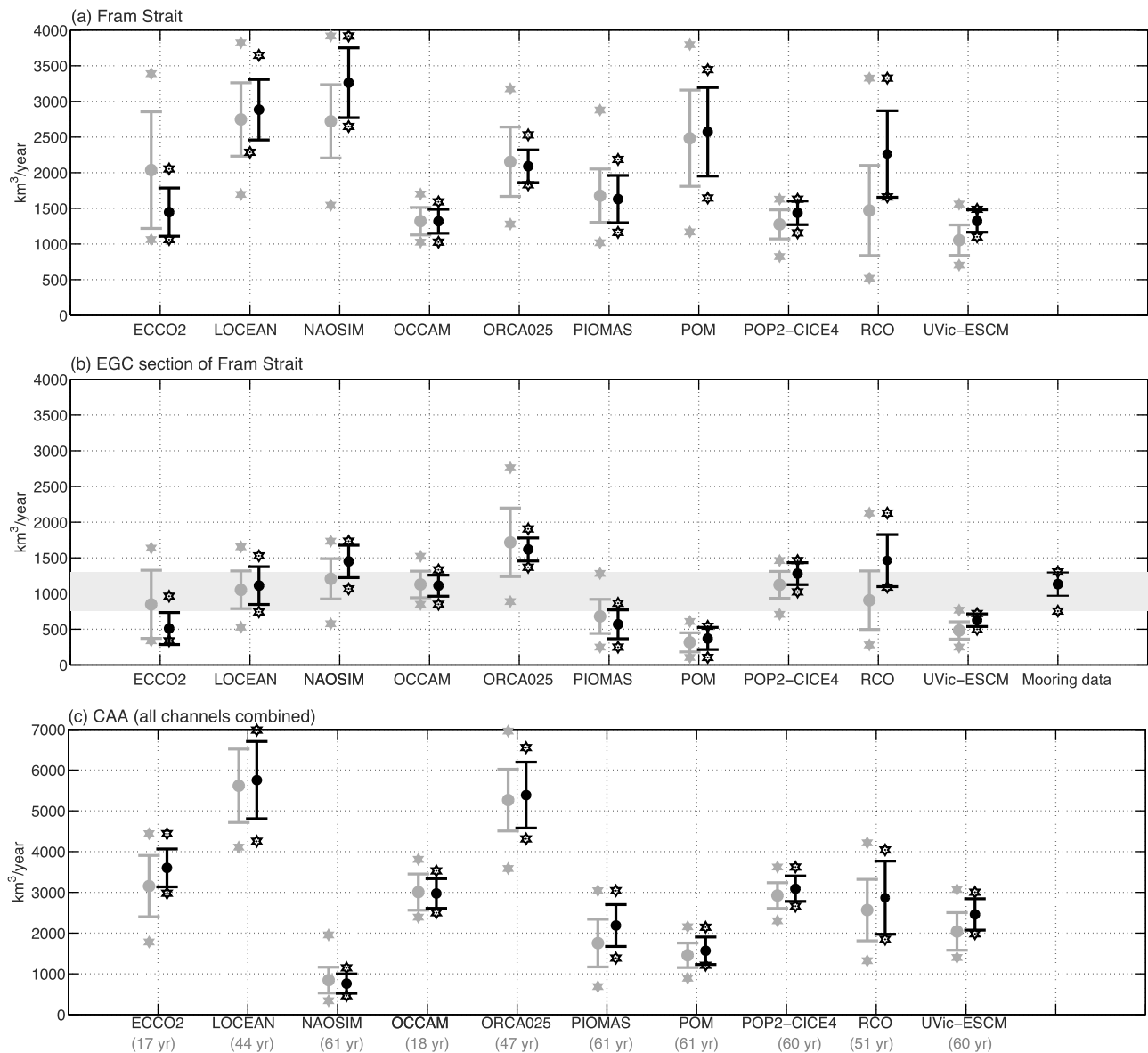


Figure 3. Standard deviation (lines), means (dots in middle of lines), and maximum and minimum values (stars) of the liquid FW export (km³/year) through (a) Fram Strait, (b) the part of Fram Strait covered by the mooring (6°W to 0°W), and (c) the CAA (combining export through all open pathways in the CAA). The 10-year averages for the maximum period of overlap (1992–2001) are shown in black, while values for the full length of the model output from each model is shown in grey, with the length of the simulation given in grey in Figure 3c on the x-axis. In Figure 3b, the mooring data from Fram Strait is shown for the 10 years of published data (1998–2008), covering the same length as the model output shown in black, but for a slightly later time period. The full range of the annual means of the mooring data is also shown as grey shading in Figure 3b, to facilitate the comparison of the model results and the mooring data for the same section of Fram Strait.

2011], this highlights the need for long-term monitoring in the Fram Strait and CAA channels.

[31] To compare the simulated FW fluxes through Fram Strait with the available mooring data from the EGC in Fram Strait (between 6°30'W and 0°W; see *de Steur et al.* [2009] for details), we obtained sub-sections of the Fram Strait transect that cover the region between 6°30'W and 0°W from the models (called “EGC” in the following). It should be noted, however, that due to the coarse resolution in some

models and the grid orientation and spacing the “EGC” model sub-sections cannot be collocated exactly to the mooring sub-section. As a result, the “EGC” sub-section in the models does not contain the EGC in all models, due to differences in the details of the flow. Despite the obvious shortcoming of looking at these “EGC” sub-sections in the simulations, we will use them in the following to see what impact it has on the results when we look only at a sub-section of Fram Strait. It also illustrates the difficulty of

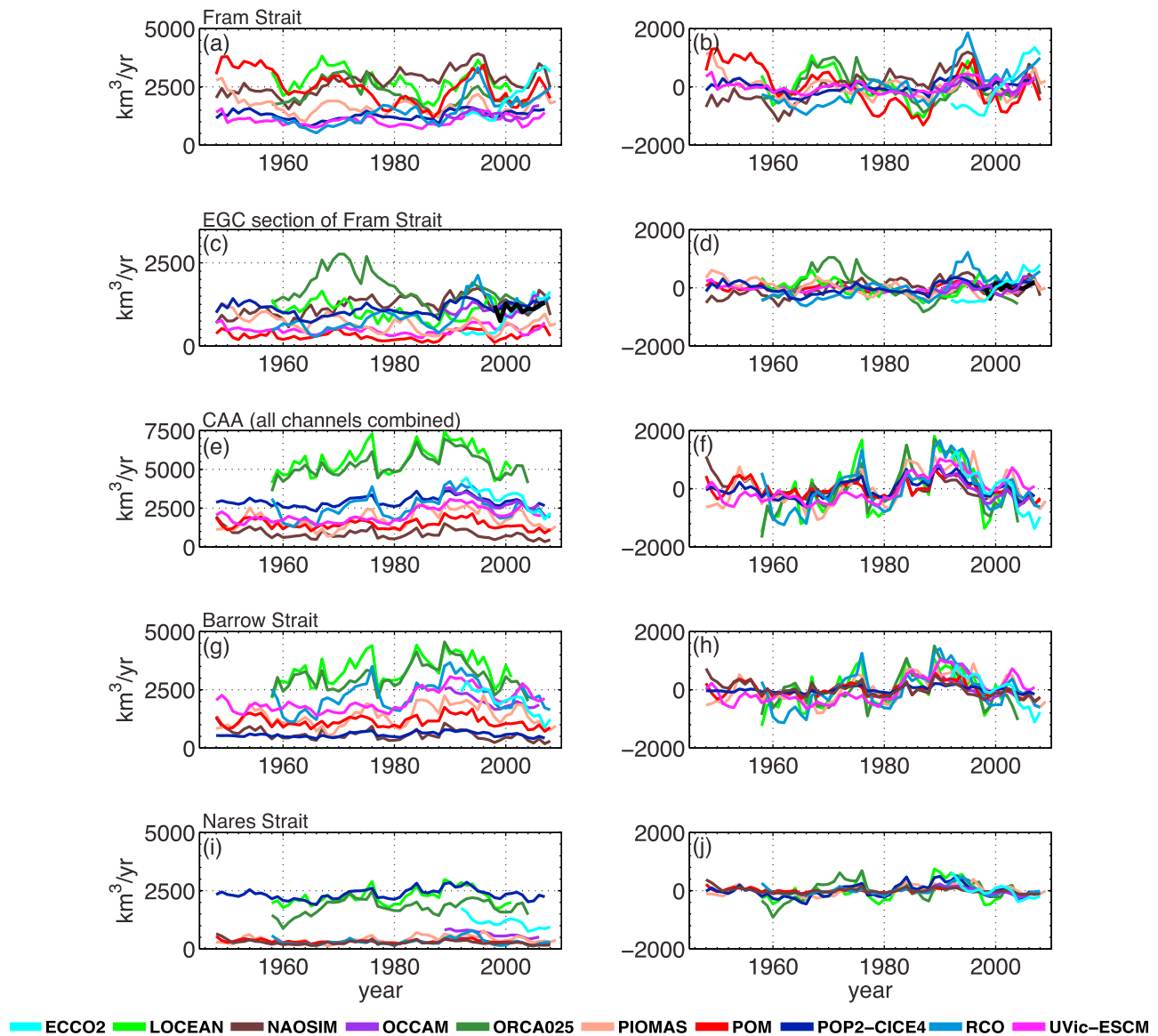


Figure 4. Simulated time series of the annual mean southward liquid FW flux and the corresponding flux anomalies (mean southward liquid FW flux removed); (a, b) flux through Fram Strait across the whole strait for the top 250 m, (c, d) flux through the Fram Strait section between 6°W and 0°W (EGC) for the top 250 m; (e, f) the liquid FW flux through all passages of the CAA; (g, h) flux through Barrow Strait; and (i, j) flux through Nares Strait. Fluxes through other CAA channels are small (if more than two channels are open in models) and are not shown. The results from ten AOMIP models are shown by colored lines, the observations (if available) are shown in black; the fluxes are relative to 34.8.

comparing mooring arrays with model sections to evaluate model transports. Looking at the “EGC” sub-sections in Fram Strait, we find that the simulated mean liquid FW export as well as its standard deviation are reduced in all models compared to the full transect across the strait (see Figures 3a and 3b). Compared to the 1998–2008 mooring-derived liquid FW export in the top 250 m, all models except POM show values that fall into the range of the mooring-derived FW export at some point in their simulation, but only a few models simulate a range of values that are close to the mooring-derived FW fluxes (see Figure 3b).

[32] For the solid FW export through Fram Strait, the simulated standard deviation of the annual mean for 1992–2001

is similar to the liquid FW export, ranging from $270\text{ km}^3/\text{yr}$ to $611\text{ km}^3/\text{yr}$. This compares well to the standard deviation of $621\text{ km}^3/\text{yr}$ and $419\text{ km}^3/\text{yr}$ obtained from the observed 5-year long time series of sea ice export through Fram Strait [Vinje *et al.*, 1998; Kwok and Rothrock, 1999], as well to the standard deviation of $286\text{ km}^3/\text{yr}$ in the 7-year long record [Kwok *et al.*, 2004].

[33] For the liquid FW export through the combined channels of the CAA over the same 10 year period (1992–2001), the models show an even larger spread in the annual mean ($760\text{ km}^3/\text{yr}$ to $5756\text{ km}^3/\text{yr}$) and the standard deviation ($178\text{ km}^3/\text{yr}$ to $948\text{ km}^3/\text{yr}$) than in Fram Strait (see Figure 3c). As the narrow channels of the CAA are

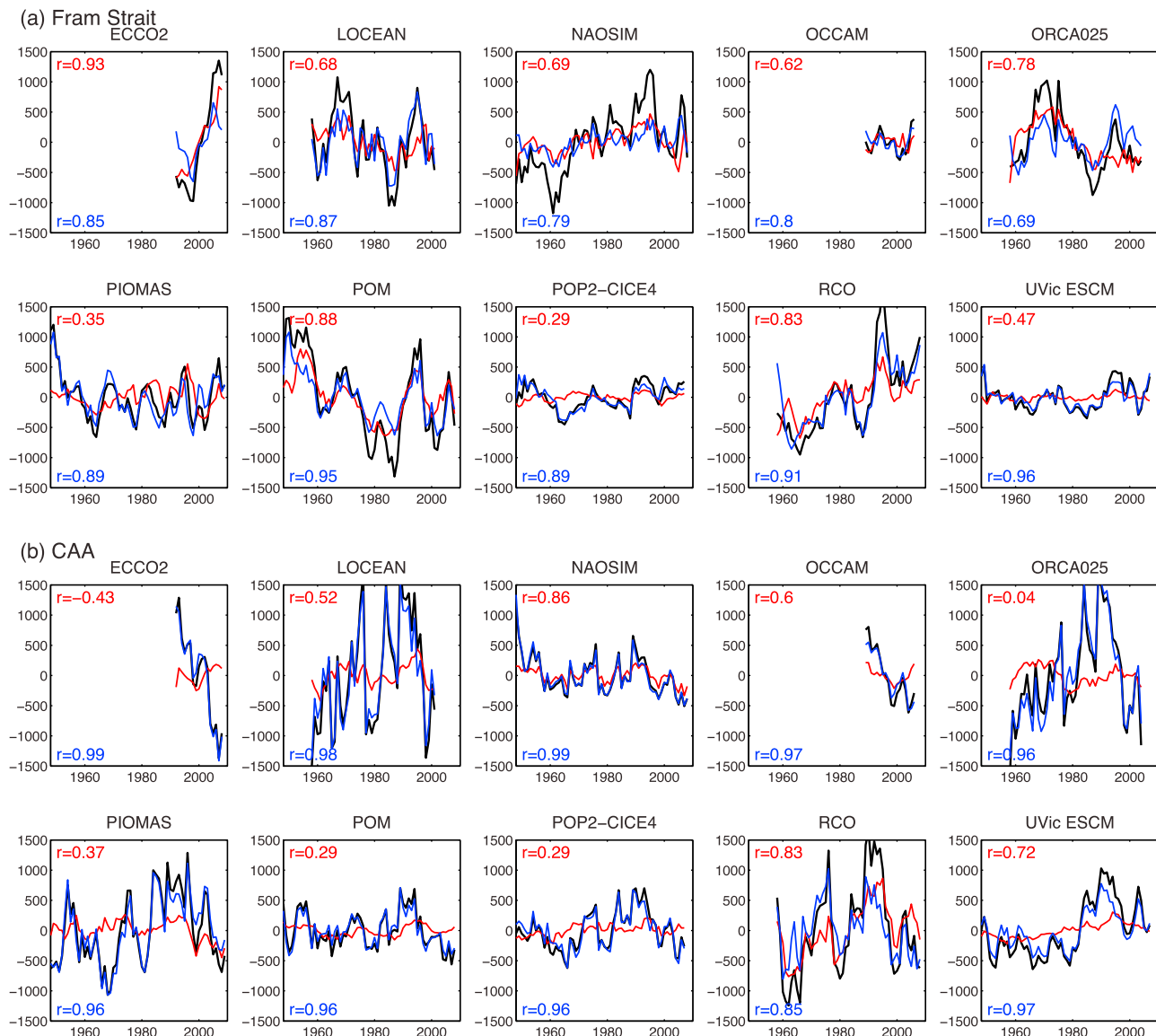


Figure 5. Simulated time series of anomalies of the annual mean southward liquid FW flux in (a) the top 250 m in Fram Strait and (b) the CAA (all channels combined). The results from ten AOMIP models are shown in different panels. The total liquid FW flux anomaly is in black, the salinity-driven FW flux anomaly is in red, and the volume-flux-driven FW flux anomaly is shown in blue. Red numbers show the correlation of the salinity driven FW flux anomaly with the total liquid FW flux anomaly, and blue numbers show the correlation of the volume driven FW flux anomalies with the total liquid FW flux anomalies. All FW fluxes are relative to 34.8. Overall this figure shows that in Fram Strait both salinity and volume flux driven FW export anomalies contribute to the total liquid FW export variability while in the CAA the volume flux driven FW export anomalies dominate the variability of the liquid FW export.

represented with different levels of accuracy due to the differences in model resolutions, this larger spread is perhaps not surprising. We cannot, however, find a robust relationship between horizontal resolution and the simulated mean or standard deviation of the liquid FW export through the CAA channels. For the solid FW export through the CAA, the standard deviation is much smaller than for the liquid FW export, and ranges from 3 km³/yr to 240 km³/yr.

5.1.2. Time Evolution

[34] In terms of the variability in the simulated FW export time series, we see a more consistent simulation of the FW

export variability in the CAA compared to Fram Strait (see Figure 4). In order to investigate the differences between the model-simulated variability in the time series of the FW export in detail, we look at the liquid FW export as well as at the contributions of volume flux and FW concentration anomalies to the interannual variability of the liquid FW export. To do this, we split the FW export (F_{FW}) into a time-mean component and three time-varying terms, following *Jahn et al.* [2010b]:

$$F_{FW} = \langle C_{FW} \rangle \langle v_{\perp} \rangle + v'_{\perp} \langle C_{FW} \rangle + C'_{FW} \langle v_{\perp} \rangle + C'_{FW} v'_{\perp}, \quad (1)$$

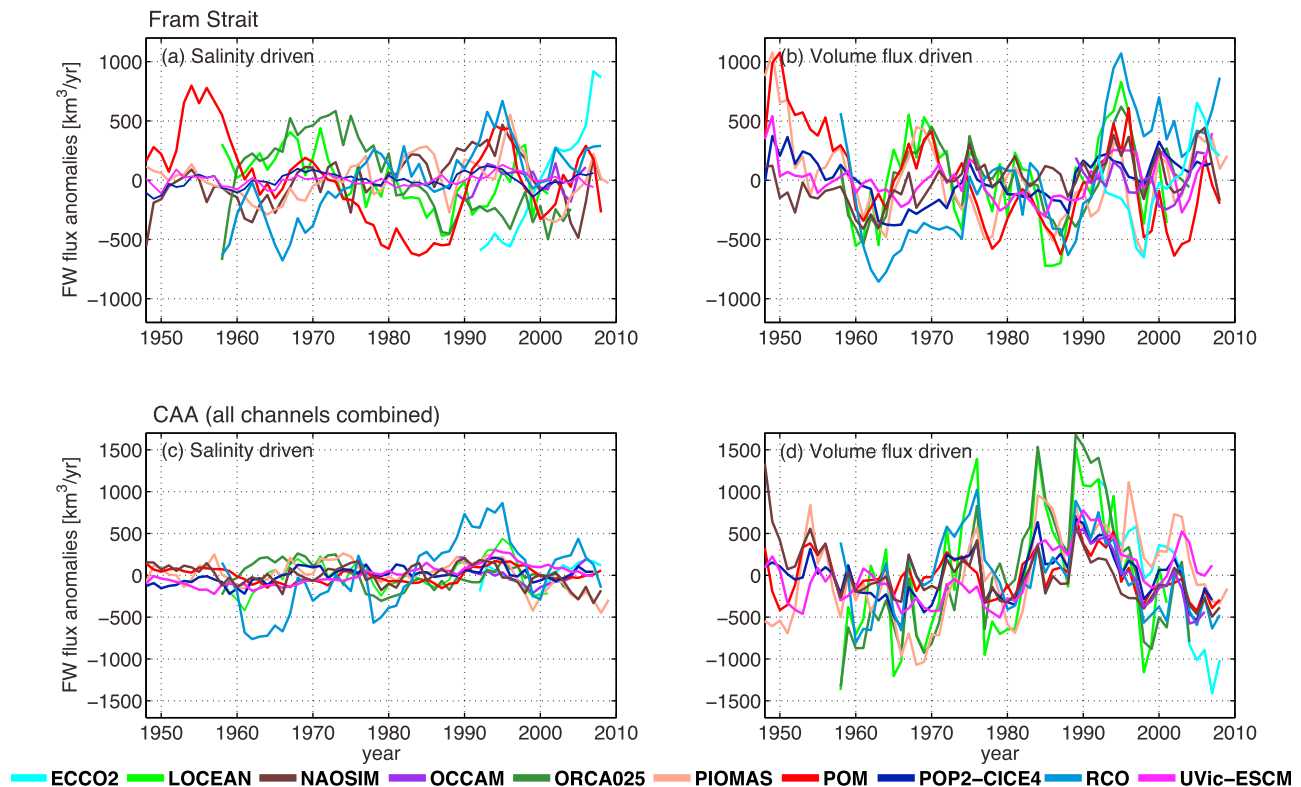


Figure 6. Simulated liquid FW export anomalies in (a, b) Fram Strait and (c, d) CAA due to salinity anomalies (left column) and volume flux anomalies (right column) for the different models. Note the much larger similarity of the volume flux driven FW export anomalies (Figures 6b and 6d) compared to the salinity-driven FW export anomalies (Figures 6a and 6c).

where v_{\perp} is the volume-flux component perpendicular to the strait and C_{FW} is the concentration of FW relative to the reference salinity. Primed variables stand for temporal anomalies and variables in brackets stand for time mean values. Accordingly, $\langle C_{FW} \rangle \langle v_{\perp} \rangle$ is the FW flux through a strait due to the mean FW concentration advected by the mean volume flux, $v'_{\perp} \langle C_{FW} \rangle$ is the FW flux due to the advection of the mean FW concentration by the volume flux anomaly, $C'_{FW} \langle v_{\perp} \rangle$ is the FW transport associated with the advection of FW concentration anomalies (due to salinity changes, called salinity-driven anomaly in the following) by the mean flow, and $C'_{FW} v'_{\perp}$ is the FW flux due to the advection of FW concentration anomalies by volume flux anomalies. As $C'_{FW} v'_{\perp}$ is very small, it is not discussed in the following.

[35] Using this approach, we find that volume flux-driven FW export anomalies dominate the FW export variability in the CAA, whereas in Fram Strait the variability of the salinity of the export generally plays a larger role (Figure 5). The lowest variability of the salinity-driven FW export anomaly is seen in the UVic ESCM and the POP2-CICE4, which also have the lowest resolution and show the largest surface salinities in the Fram Strait cross section (not shown). We also find that the volume flux driven FW export anomalies show a better agreement among the different models than the salinity-driven FW export anomalies (Figure 6). The better agreement of the simulated liquid FW export through the CAA than through Fram Strait among models is therefore due to the larger influence of the volume

flux-driven FW export anomalies in the CAA and the relative similar variability of the latter in the different models.

[36] In general, the models agree on the timing of most liquid FW export maxima and minima, even in Fram Strait, due to the influence of the volume-flux driven FW export anomalies (see Figures 4b and 4f, and Figure 6). An exception is the ECCO2 model, which in Fram Strait shows a variability that is different from the other models, for unknown reasons. Given that most models suggest an important contribution of salinity-driven FW export anomalies to the variability of the Fram Strait liquid FW export, the inconsistency of salinity variations among models is an important problem that needs to be investigated in the future with coordinated model experiments.

[37] The variability of the solid FW export through Fram Strait shows the best model-to-model agreement of all time series we investigated (Figure 7), as shown by the correlation among the time series from different models (with a mean correlation coefficient of $r = 0.70$). Compared to the short observational time series (from satellite data and upward looking sonars, as described in *Kwok et al.* [2004]), the variability of the models also matches that of the observations very well, with peaks in 1992 and 1994/95.

[38] In terms of similar variability in different straits, we find that the variability of the annual mean liquid FW export in Barrow and Nares Strait is highly correlated in all models with at least two CAA passages (with r -values between $r = 0.67$ and $r = 0.92$, statistically significant at the 99% confidence level; see also Figure 4). An exception is the

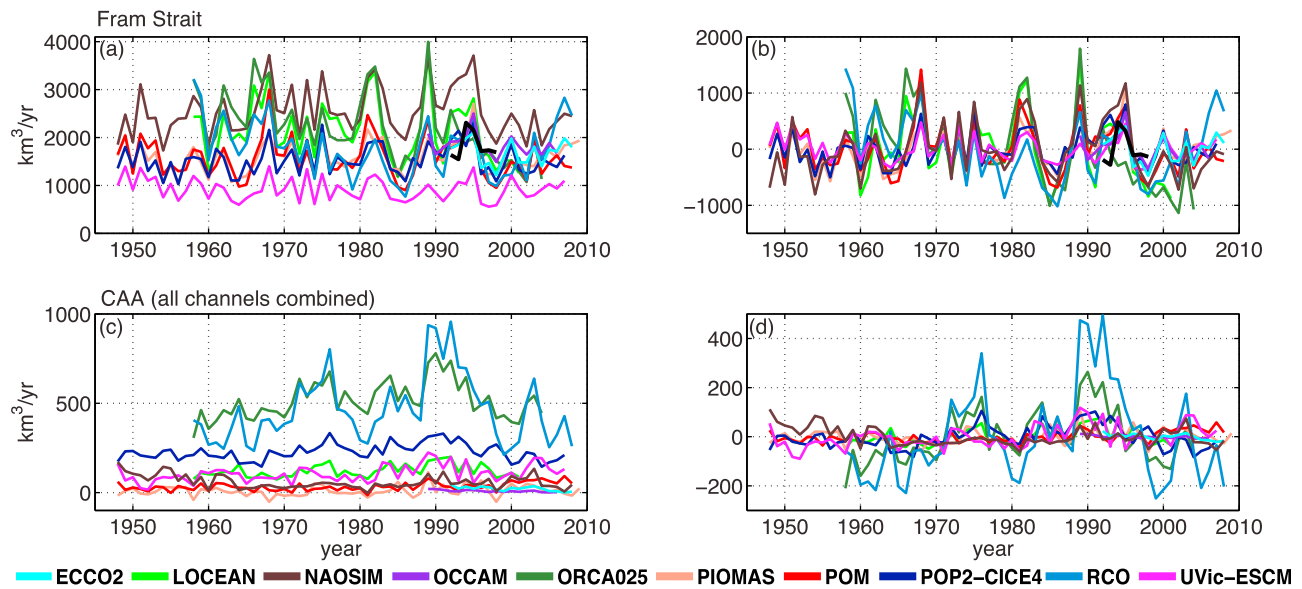


Figure 7. Simulated time series of the annual mean net solid FW flux and the corresponding flux anomalies (mean solid FW flux removed) through (a, b) Fram Strait and (c, d) the CAA (all passages combined). In addition to the models, the black line shows the observational time series of ice volume flux through Fram Strait from *Kwok et al.* [2004] for 1992–1998, derived from passive microwave satellite data (for the ice motion) and upward looking sonar (for the ice thickness). We used a salinity of 4 and a ice-density of 910 kg/m^3 to convert these ice volume fluxes into solid FW fluxes. All fluxes are relative to 34.8 and positive values indicate southward FW fluxes.

ORCA025 model, where no significant correlation at any lag is found between the liquid FW export through these two straits, for unknown reasons. We do not see a consistent correlation between the liquid FW exports east and west of Greenland, with some models showing a lagged correlation at 3–5 years or 0–1 years while others show no statistically significant correlations at any lag. As observational time series are presently too short to investigate the correlation between the liquid FW export through the Fram Strait and the CAA, the question whether the liquid FW exports east and west of Greenland are physically linked or not stays unanswered and the possible mechanisms behind this link need to be further investigated in the future.

5.1.3. FW Storage Variability

[39] Given the large differences in the magnitude of the FW storage integrated over the Arctic, the comparison of FW storage anomalies, rather than the total FW storage time series, is more instructive, and shows that the amplitude of liquid FW storage anomalies are different among models (Figure 8). Certain consistent features, however, appear in most of the simulations. These features include a maximum in the liquid FW storage during the late 1960s and in the early 1980s, a minimum during the late 1970s and the mid-to-late 1990s, and an increase in the FW storage after 1998 (Figures 8b and 8d). Some models also show a maximum around 1990, which can be larger or smaller than the one in the early 1980s. The increase in the liquid FW storage in the Arctic since the late 1990s, which is shown in seven of the ten models (all except UVIC ESCM, RCO, ECCO), is in agreement with recent results from *McPhee et al.* [2009], *Proshutinsky et al.* [2009], and *Rabe et al.* [2011], which all show a strong increase in the liquid FW storage in the Arctic Ocean since the mid-to-late 1990s. The reasons for the

differences in simulated liquid FW storage between models are not clear. For example, we do not see a consistent impact of horizontal resolution or restoring. To identify which factors contribute to the differences in the simulations, coordinated studies are needed, which could investigate the impact of the use of different atmospheric forcing data, restoring strengths, and model physics.

[40] For the solid FW storage, models with the thinnest ice in the Arctic (POP2-CICE4 and UVic ESCM) show the smallest amplitude in their variability, as well as less agreement with the interannual variability of models with more sea-ice (Figure 8d). Overall, the variability of the solid FW storage among the different models has a smaller amplitude and shows a higher frequency than the variability of the liquid FW storage. Furthermore, compared to the liquid FW storage variability, the solid FW storage variability shows a better agreement across the different models, as was already seen for the solid and liquid FW exports. Hence, it appears that the most important feature that needs improvement in some models in order to simulate the solid FW storage better is a more realistic simulation of the ice thickness in the Arctic. It is important to note that the differences in the ice thickness might not be due to the ice models themselves, but could be caused by the atmospheric forcing used to force the models and the tuning of models to this forcing (as already discussed in section 4.2).

6. Seasonal Cycle of FW Export

6.1. Fram Strait

[41] The models simulate a minimum in the seasonal cycle of the liquid FW export through Fram Strait in May and/or June and the maximum between September and November

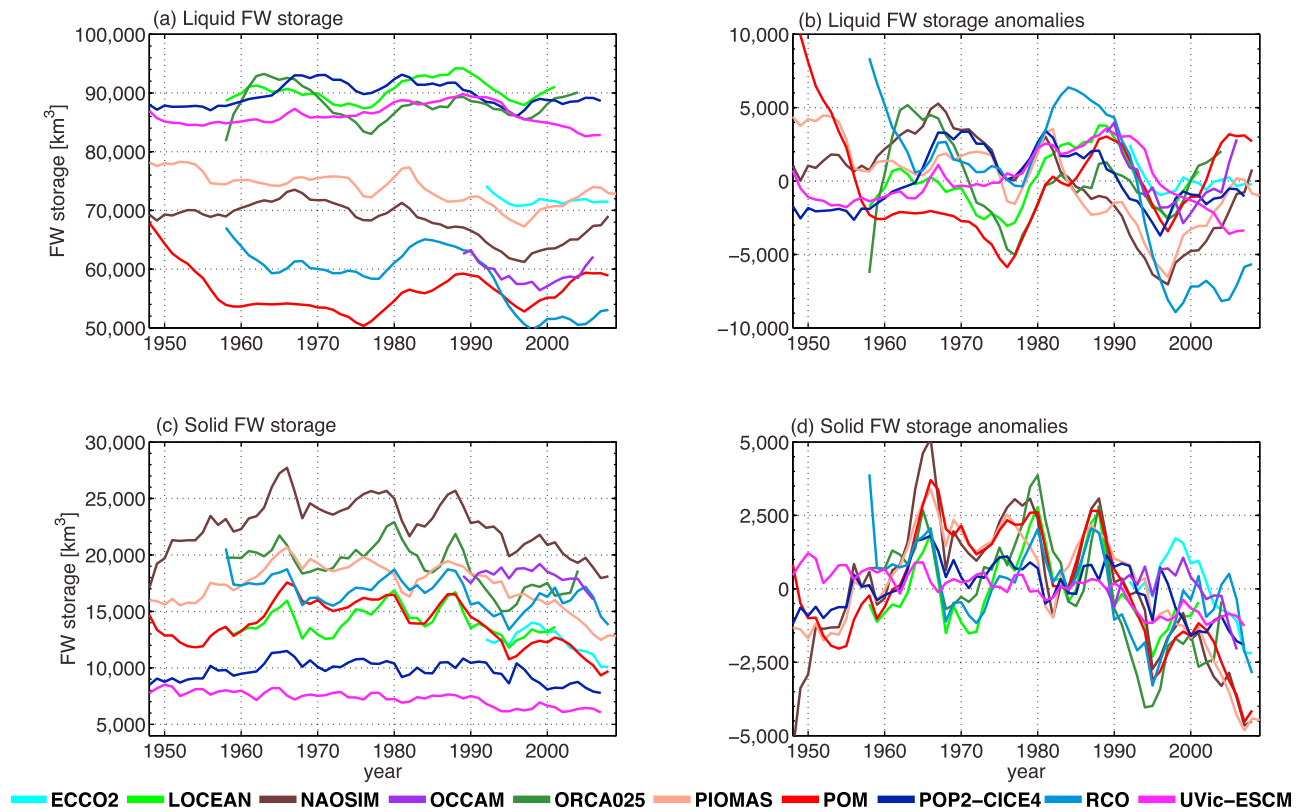


Figure 8. Simulated time series of the (a) liquid and (c) solid FW storage in the Arctic (relative to 34.8, averaged over the top 250 m) and (b, d) the corresponding anomalies (mean FW storage removed). The solid FW storage includes FW from the snow on the ice as well as from the ice. Note the much better agreement of the variability of the solid FW storage anomalies compared to the liquid FW storage anomalies.

(Figure 9a). Focusing on the EGC-sub-section of Fram Strait (Figure 9d), we find that the models show a much less consistent picture of the seasonal cycle. This is mainly due to the volume flux driven FW export anomalies in the sub-section (Figure 9b versus 9e), caused by the fact that the EGC sub-section from the models is not necessarily where the EGC is located in the individual models (as already discussed in section 5.1.1). The shape of the seasonal cycle of the salinity-driven FW export anomalies is less affected by taking only a sub-section and mainly shows a reduction of the amplitude (Figure 9c versus 9f), suggesting that the seasonal cycle of the salinity signal of the outflow is similar on the shelf and in the EGC, at least in the models.

[42] Compared with the new mooring-derived seasonal cycle of the liquid FW export in the EGC in Fram Strait (L. de Steur et al., manuscript in preparation, 2012; see data description in section 3), the simulated seasonal cycle of the Fram Strait liquid FW export is largely within the uncertainty range of the observational data (see Figures 9a and 9d). The uncertainty range of the data combines the uncertainty based on the different strength of nudging towards hydrography between 50 m and the surface (see section 3) and the standard deviation between 2002–2007. The models are also largely within the observational uncertainty range if we use the full Fram Strait sections from the

models, which we will use in the following for the comparison as it better represents the model simulated seasonal cycle of the outflow than the flux through the (arbitrary) EGC sub-sections. We find that the timing of the seasonal minimum differs between the simulations and the mooring-derived estimate (see Figure 9a), with the simulated minimum in May being outside the uncertainty range of the mooring data, which shows a minimum in June–July. For the maximum, the agreement between the mooring-derived estimate and most of the simulations is better, with a maximum in September.

[43] The analysis of the volume and salinity-driven FW export anomalies in the strait (Figures 9b and 9c) shows that the FW export minimum is caused by the concurrent decline of the volume export from February to August and the export of saltier water in April–May in the models or June–July in the mooring-derived estimate. The difference in the timing of the minimum is mainly due to the increase in the volume flux in May and the decline of the volume flux until July in the mooring-derived estimate, which are both not simulated by any of the models. However, given the uncertainty range of the mooring-derived estimate, it is unclear if these features are real. The fall maximum in the FW export is also due to a concurrent effect of the volume export increase from summer to winter and freshening of the upper ocean in fall due to sea ice melt (Figures 9b and 9c).

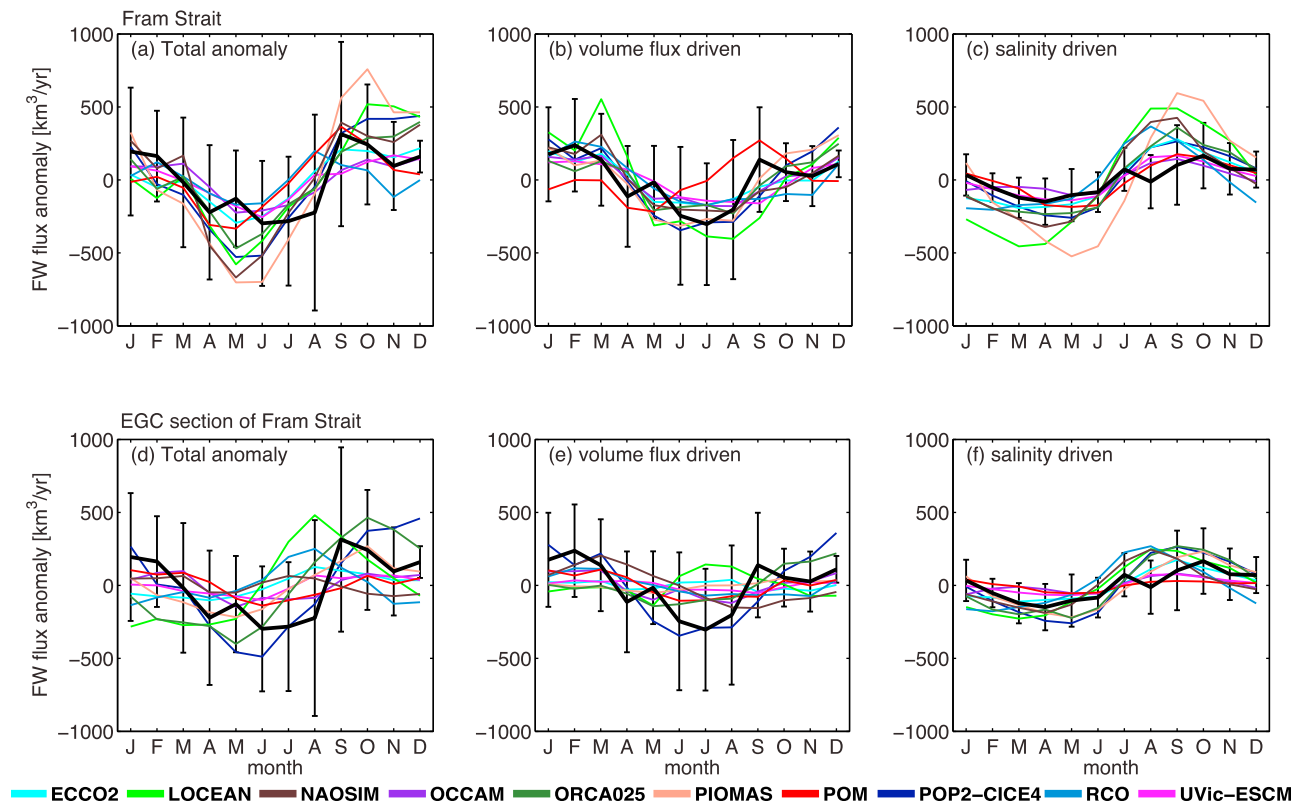


Figure 9. Seasonal cycle of the (a, d) liquid FW export in the top 250 m, (b, e) volume flux driven FW export anomaly in that layer, and (c, f) salinity-driven FW export anomaly as simulated by AOMIP models for the full Fram Strait section (Figures 9a–9c) and in the EGC sub-section (Figures 9d–9f, 0 to 6°W). All simulated fluxes are averaged over 1992–2001, and show the seasonal anomaly compared to the annual mean. In all plots the seasonal cycle of the mooring-derived seasonal liquid FW export anomaly (averaged over 2002–2007) is shown in black, with error bars showing the uncertainty in the estimate, based on the different strength of nudging towards hydrography in the surface layer and the standard deviation.

Table 4. Amplitude of the Seasonal Cycle of the Liquid and Solid FW Export (in km³/year) Through Fram Strait, the Mooring-Covered Region of Fram Strait, Barrow and Nares Strait, and All CAA Channels Combined^a

	Observations	ECCO2	LOCEAN	NAOSIM	OCCAM	ORCA025	PIOMAS	POM	POP2/CICE4	RCO	UVIC-ESCM
Fram Strait liquid FW	unknown	510	1097	1062	372	867	1460	698	966	369	424
EGC part of Fram Strait liquid FW	612	228	764	138	245	865	486	243	947	386	169
Fram Strait solid FW	2109 ⁺ /2765 ^o	2147	2903	3481	1977	1804	2776	1807	3399	1664	1579
Barrow Strait liquid FW	1722 ± 20%	1111	1300	434	377	1623	1486	555	312	842	262
Nares Strait liquid FW	unknown	487	584	199	392	820	236	177	701	244	–
CAA liquid FW	unknown	1455	1476	568	763	2196	1722	561	959	1079	262
CAA solid FW	115	111	180	220	48	454	303	83	131	268	162

^aAll simulated fluxes are for 1992–2001, compared with observational fluxes for any available period. The mooring-derived FW flux for the EGC in Fram Strait is the new mooring-based estimate shown in Figure 9 (L. de Steur et al., manuscript in preparation, 2012), averaged over 2002–2007. As there are no observational estimates for the seasonal cycle of the FW flux on the East Greenland shelf in Fram Strait due to the ice conditions there, the total magnitude of the seasonal cycle for Fram Strait is still unknown. The estimate of the seasonal cycle of the solid FW export through Fram Strait is derived from the average amplitude between 1991–1995 in the data of Vinje et al. [1998], denoted by a superscript plus sign and Kwok and Rothrock [1999], denoted by a superscript o. The observational estimate of the seasonal cycle of the liquid FW export through Barrow Strait is based on 11 years (1999–2009) of data from Lancaster Sound (S. Prinsenberg, personal communication, November 2011, updated from Prinsenberg et al. [2009]). Note that the uncertainty in this data is approximately 20%. For Nares Strait, there is no credible quantitative estimate for the seasonal variation in the liquid FW export through Nares Strait, as most of the seasonality occurs in the uppermost 40 m, which are not accessible to instruments on moorings, and ice conditions preclude CTD measurements during most of the year (H. Melling, personal communication, December 2011). The estimate of the seasonal cycle of the solid CAA FW export is a rough estimate based on values for the ice volume export from Kwok [2005] for Nares Strait and from Prinsenberg and Hamilton [2005] for Lancaster sound.

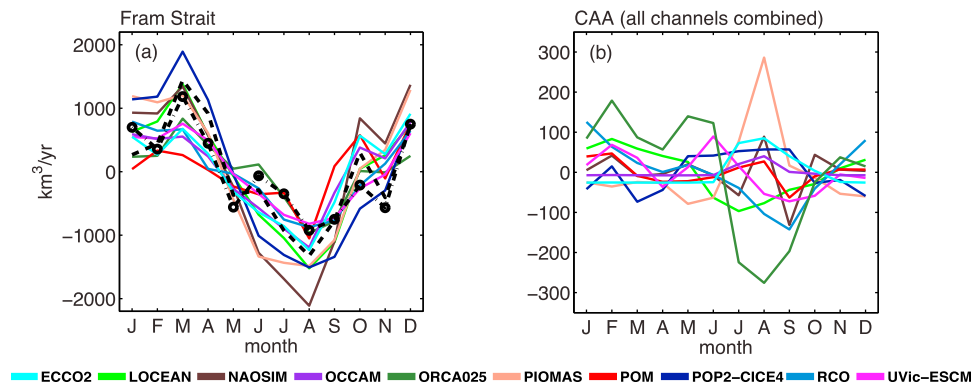


Figure 10. Seasonal cycle of the solid FW export through (a) Fram Strait and (b) all CAA channels combined (in km^3/yr). All simulated fluxes are averaged over 1992–2001 and show the seasonal anomaly compared to the annual mean. The black lines show available data for the seasonal anomaly in Fram Strait, derived from passive microwave satellite data (for the ice motion) and upward looking sonar (for the ice thickness). The black dashed line shows the data from *Vinje et al.* [1998], and the dashed black line with circular markers shows the data from *Kwok and Rothrock* [1999], both averaged over 1991–1995.

[44] The seasonal cycle of the solid FW export through Fram Strait is much larger than the seasonal cycle of the liquid FW export in all models (by a factor of 2–6; see Table 4) and has a minimum in August and a maximum in

March (Figure 10a). Compared to the available observational data for the solid FW export (calculated from satellite data and upward looking sonars; see *Vinje et al.* [1998] and *Kwok and Rothrock* [1999]), the models agree quite well

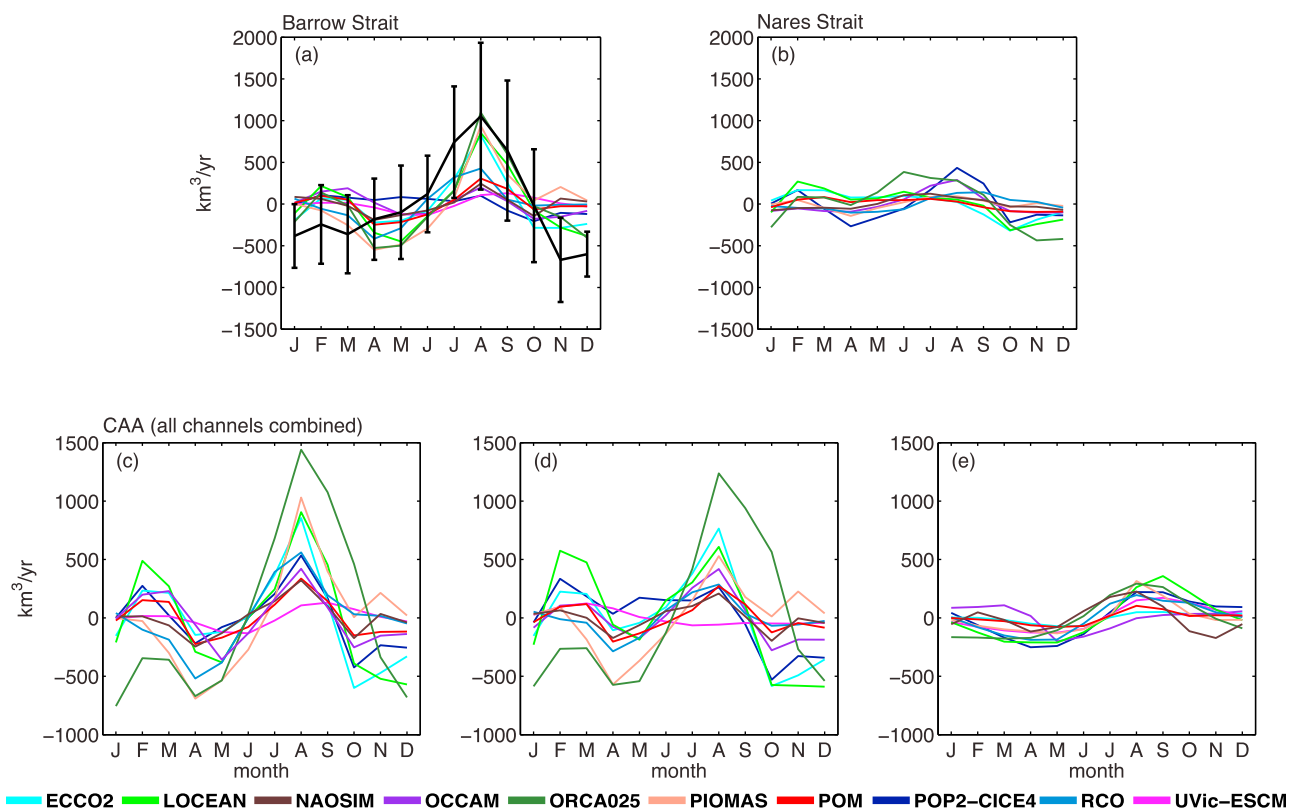


Figure 11. Seasonal cycle of the liquid FW export through (a) Barrow Strait, (b) Nares Strait, (c) all CAA channels combined, (d) the volume flux-driven FW export anomaly for all CAA channels, and (e) the salinity driven FW export anomaly for all CAA channels. All simulated fluxes are averaged over 1992–2001 and show the seasonal anomaly compared to the annual mean. Mooring-derived estimates of the seasonal anomaly of the liquid FW export through Lancaster Sound (S. Prinsenberg, personal communication, November, 2011, updated from *Prinsenberg et al.* [2009]) are shown in black, with error bars showing the standard deviation of the seasonal cycle over the 11 years of available data (1999–2009).

with the observations, even though the amplitude of many models is larger than shown in the observational data (Figure 10a and Table 4). The shape of the seasonal cycle of the solid FW export is due to the seasonal cycle of the wind forcing, which also impacts the seasonal volume-flux driven FW export anomaly, as well as due to the seasonal cycle of the ice thickness and concentration (not shown). As seen for the interannual variability, the agreement among models on the seasonal cycle of the solid FW export through Fram Strait is again much better than for the liquid FW export (Figure 10a).

6.2. CAA

[45] In the CAA, the models generally show a larger seasonal cycle of the liquid FW export in Barrow Strait compared to Nares Strait (Figures 11a–11b and Table 4), in agreement with observational estimates (see caption of Table 4 for references to the data). An exception is the POP2-CICE4 model, which shows a larger seasonal cycle in Nares Strait, in addition to its overall larger liquid FW export there.

[46] In contrast to the seasonal cycle of the liquid FW export through Fram Strait, the simulated seasonal cycle in the CAA has two peaks, a smaller one in February (extending into March in some models) and a larger one in August (Figure 11c), in general agreement with observational data from Lancaster Sound (S. Prinsenberg, personal communication, November 2011, updated from *Prinsenberg et al.* [2009]). An exception is the secondary minimum in February–March, which is more pronounced in the model simulations. Furthermore, the models show higher fluxes in November and December than seen in the mooring data, potentially due to the lack of land fast ice during winter in most models (see next paragraph), which would limit the outflow through the CAA channels. In the simulations, we find that most of the seasonal cycle of the liquid FW export through the CAA is due to seasonal changes in the volume outflow through the channels of the CAA, which also cause the two-peak pattern (Figure 11d). Seasonal salinity variations are small, but contribute to the larger peak in August (Figure 11e).

[47] The seasonal cycle of the solid FW export in the CAA is small in most models (see Table 4 and Figure 10b). The shape of the seasonal cycle, however, is not very consistent among models, with some showing a peak between July and September while others show a peak in winter and a minimum in August to September. A small peak in the summer months agrees with limited observational data from Nares Strait, which show a peak in the ice area flux in July and August after the break-up of the sea ice and an almost vanishing ice flux between late November and March due to land fast ice [*Kwok*, 2005], with similar conditions in Lancaster Sound [*Prinsenberg and Hamilton*, 2005]. Only two of the investigated models, ECCO2 and OCCAM, show a vanishing ice flux between November and March as described in the observations, while all other models show some ice flux during the winter and spring (not shown), indicating that the ice is not land-fast in most models and probably flows too freely through the CAA. This also impacts the outflow of the water under the ice, as seen by the too large liquid FW export during winter compared to the mooring data from Lancaster sound.

Hence, improved simulations of the ice conditions in the CAA should be an important priority in order to improve model simulations of the Arctic FW budget.

7. Summary

[48] We found that eight of the ten models show the largest net liquid FW export through the CAA, with less net liquid FW export through Fram Strait, whereas all models agree that the solid FW export is larger through Fram Strait than through the CAA. Overall, half the models show the largest total net FW export (solid plus liquid) occurring through Fram Strait while the other half shows the largest total FW export through the CAA channels. In addition, eight of the nine models with at least two open CAA channels show a larger liquid FW export through Barrow Strait than through Nares Strait, in agreement with the available observations.

[49] In terms of the variability of the FW export, the models also show large differences, both in terms of the magnitude of the standard deviation and the time series variability. The best model-to-model agreement is found for the simulated interannual solid Fram Strait FW export variability, in spite of model-to-model differences in the mean solid FW export. The two models that do not agree as well with the others are the models that simulate a too thin ice cover, highlighting the importance of a realistic sea-ice thickness simulation.

[50] For the liquid FW export, we find that the model-to-model agreement is better in the CAA than in Fram Strait. This is caused by the more dominant role of volume-flux driven FW export anomalies in the CAA in all models, while salinity driven FW export anomalies are more important in Fram Strait. Indeed, the volume-flux driven FW export anomalies show a generally better agreement among the models than salinity-driven FW export anomalies. Hence, the inconsistent simulation of the salinity of the outflow degrades the model-to-model agreement. In order to improve simulations of the liquid FW export and make the results less model dependent, the most important issue that needs to be resolved is the simulation of the variability of the salinity field in the Arctic. The simulated variability of the annual mean liquid FW export in Barrow and Nares Strait is highly correlated in all models with at least two CAA passages, in agreement with observations.

[51] For the FW storage, the solid FW storage variability is more consistent in the different models than the liquid FW storage variability, due to the model differences in both the mean salinity field and the temporal and spatial variability of the salinity field. The main difference in the FW storage variability is due to differences in the simulated mean ice thickness. As discussed for the example of the POP2-CICE4 compared to the coupled CCSM4, the sea ice thickness simulation can be strongly affected by the atmospheric forcing (and the tuning to this forcing), rather than only by the sea-ice model itself. More studies on the sensitivity of models to different forcing would therefore be welcome.

[52] Compared to the interannual variability, we find that the models show a better agreement on the seasonal cycle of the liquid FW export from the Arctic than on the interannual variability. In the CAA the seasonal cycle of the liquid FW export has two peaks and is mainly caused by seasonal

volume-flux changes. In eight of the nine models with more than one channel in the CAA, Barrow Strait shows a larger seasonal cycle of the liquid FW export than Nares Strait, in agreement with the limited available observations. In Fram Strait the seasonal cycle of the salinity of the outflow plays a larger role than in the CAA. Compared to the mooring data in the EGC, the simulated seasonal cycle of the liquid FW export is mainly within the uncertainty range of the observations and shows the same general shape as observed, but observations of the liquid FW flux on the East Greenland shelf are needed in order to establish the total amplitude of its seasonal cycle.

[53] The simulated seasonal cycle of the solid FW export through Fram Strait shows a good model-to-model agreement as well as matching the shape of the observational estimates. All of the models furthermore agree that the amplitude of the seasonal cycle of the solid FW export through Fram Strait is much larger than that of the liquid FW export, ranging from a factor of two to a factor of six times the amplitude of the seasonal cycle of the liquid FW export. In the CAA, all models agree that the seasonal cycle of the solid FW export is very small, but there is disagreement on the shape of the seasonal cycle of the solid FW export, due to a lack of land-fast ice in many of the models. This highlights another area where model improvements are needed.

8. Conclusions

[54] We compared hindcast simulations of the Arctic FW budget, storage, and export from ten ocean-sea ice models. The simulations from these models were existing model simulations, performed with uncoordinated model forcing, set-up, model physics, and length of the integrations. We focused our analysis mainly on 1992–2001, the longest period of overlap among the simulations. The analysis showed that the investigated models overall agree on the source and sink terms of the climatological Arctic FW budget. The simulated mean fluxes and the details of the interannual and seasonal variability, however, were found to vary among models. Due to a lack of long term observations of the FW export through the different straits, we can not determine which simulations are closest to reality, but can only point out the features that the ten investigated models agree or disagree on. This is important, as it highlights aspects of the Arctic FW budget that are more consistently simulated in the models, giving model studies of these aspects in just one model more credibility. However, for many aspects of the Arctic FW budget, for example the liquid FW export through Fram Strait, the models do not agree on the means or the variability, making single-model studies problematic, as the results might be strongly model dependent. In the investigated models, the most robust features of the simulations were the variability (but not the means) of the solid FW export through Fram Strait (both seasonally and interannually) and the solid FW storage in the Arctic. The next best agreement among models was seen for the interannual variability of the liquid FW export through the CAA as well as for the seasonal cycle of the liquid FW export through Fram Strait and the CAA. The least good agreement was seen for the variability of the liquid FW export through Fram Strait and the liquid FW storage in the

Arctic, which was impacted by large disagreements on the variability of the salinity field.

[55] As we used existing simulations, sensitivity studies were not possible, precluding us from determining the reasons for the differences among simulations. From the existing simulations we have to conclude that model resolution, often suggested as one of the main reasons for model differences, did not show a clear relationship to the means or the variability of the FW fluxes. In fact, models with coarser resolutions often had similar net fluxes as higher resolution models, even though the details of the flow were not resolved in the coarser resolution models. A detailed sensitivity study with some of the investigated models is needed to determine the reasons for the surprisingly large differences in the simulated interannual variability of the liquid FW export through Fram Strait and the liquid FW storage.

[56] Overall, we conclude that a better simulation of salinity variability is the most important improvement needed to reconcile model differences and to advance our understanding of the liquid FW export from the Arctic through model studies. Furthermore, the capability of models to simulate land fast ice needs to be improved in order to better resolve the flow of water and ice through the channels of the CAA. In order to validate future models and to improve our understanding of the dynamics of the FW export, simultaneous long-term monitoring in the Fram Strait and CAA channels is needed. Furthermore, flux measurements on the East Greenland shelf in Fram Strait and in the surface layer of Nares Strait are needed to better constrain the seasonal cycle of the liquid FW export through these straits. Finally, the atmospheric forcing used to force ocean-ice models needs to be improved further, as some of the differences among the simulations might be due to the prescribed forcing, rather than to the ocean-ice models themselves.

[57] **Acknowledgments.** The manuscript was inspired by discussions at the annual Arctic Ocean Model Intercomparison Project (AOMIP) workshops, and we are thankful to AOMIP (funded by the National Science Foundation Office of Polar Programs, award ARC-0804010) for travel support to attend AOMIP meetings and for covering the publications fees. We thank all AOMIP participants for the discussions and feedback that helped to shape and improve the work presented in this manuscript, and especially Rüdiger Gerdes (AWI) and Cornelia Köberle (AWI) for discussions of the initial design of the study, as well as Andrey Proshutinsky (WHOI) for acting as editor. We also want to thank Humfrey Melling for discussions about the mooring data from Nares Strait and Simon Prinsenberg for sharing the FW fluxes calculated from the moorings in Lancaster Sound with us and for feedback on the manuscript. Comments from Marika Holland also helped to improve an earlier version of the manuscript and are much appreciated. We also thank two anonymous reviewers for their constructive and detailed comments that helped us to further improve the manuscript. Alexandra Jahn was supported through a Postdoctoral Fellowship from the Advanced Study Program at the National Center for Atmospheric Research (NCAR). NCAR is sponsored by the National Science Foundation. The POP2-CICE simulation was performed by S. Yeager (NCAR) as part of the CORE-II suit of simulations, using CISL computer resources. At the National Oceanography Centre (NOC) Southampton (Yevgeny Aksenov and Beverly de Cuevas) this study was funded by the UK Natural Environment Research Council as a contribution to the Marine Centres' Strategic Research Programme Oceans2025. NOC also acknowledges the use of UK National High Performance Computing Resource. Per Pemberton was supported by the project "Advanced Simulation of Arctic climate change and impact on Northern regions" (ADSIMNOR, 214-2009-389) funded by the Swedish Research Council for Environment, Agricultural Sciences and Spatial Planning (FORMAS). Jinlun Zhang was supported by NSF (grants ARC-0901987 and ARC-0908769) during his contribution to this manuscript. The ORCA025 simulation has been carried out within the DRAKKAR project, and was run at the IDRIS CNRS-GENCI computer center in Orsay, France, by J.M. Molines. Work performed at LOCEAN was partly supported by the European

Community FP7 through the THOR project under grant agreement GA212643. Computing resources have been provided by the French “Institut du Développement et des Ressources en Informatique Scientifique” (IDRIS). M. Karcher and F. Kauker are grateful for funding support from the project “The North Atlantic as Part of the Earth System: From System Comprehension to Analysis of Regional Impacts” from the German Federal Ministry for Education and Research, BMBF.

References

- Aagaard, K., and E. C. Carmack (1989), The role of sea ice and other fresh water in the Arctic circulation, *J. Geophys. Res.*, *94*(C10), 14,485–14,498, doi:10.1029/JC094iC10p14485.
- Aagaard, K., J. H. Swift, and E. C. Carmack (1985), Thermohaline circulation in the Arctic Mediterranean seas, *J. Geophys. Res.*, *90*(C7), 4833–4846, doi:10.1029/JC090iC03p04833.
- Adcroft, A., C. Hill, and J. Marshall (1997), Representation of topography by shaved cells in a height coordinate ocean model, *Mon. Weather Rev.*, *125*, 2293–2315, doi:10.1175/1520-0493(1997)125<2293:ROTBSC>2.0.CO;2.
- Aksenov, Y., S. Bacon, A. C. Coward, and A. J. G. Nurser (2010a), The North Atlantic inflow to the Arctic Ocean: High resolution model study, *J. Mar. Syst.*, *79*(1–2), 1–22, doi:10.1016/j.jmarsys.2009.05.003.
- Aksenov, Y., S. Bacon, A. C. Coward, and N. Holliday (2010b), Polar outflow from the Arctic Ocean: A high resolution model study, *J. Mar. Syst.*, *83*(1–2), 14–37, doi:10.1016/j.jmarsys.2010.06.007.
- Aksenov, Y., V. Ivanov, G. Nurser, S. Bacon, I. Polyakov, A. Coward, A. Naveira-Garabato, and A. Beszczynska-Möller (2011), The Arctic circumpolar boundary current, *J. Geophys. Res.*, *116*, C09017, doi:10.1029/2010JC006637.
- Antonov, J. I., R. A. Locarnini, T. P. Boyer, A. V. Mishonov, and H. E. Garcia (2006), *World Ocean Atlas 2005*, vol. 2, *Salinity*, NOAA Atlas NESDIS 62, edited by S. Levitus, 182 pp., U.S. Govt. Print. Off., Washington, D. C.
- Arzel, O., T. Fichefet, H. Goosse, and J.-L. Dufresne (2008), Causes and impacts of changes in the Arctic freshwater budget during the twentieth and twenty-first centuries in an AOGCM, *Clim. Dyn.*, *30*, 37–58, doi:10.1007/s00382-007-0258-5.
- Barnier, B., et al. (2006), Impact of partial steps and momentum advection schemes in a global ocean circulation model at eddy permitting resolution, *Ocean Dyn.*, *56*, 543–567, doi:10.1007/s10236-006-0082-1.
- Barnier, B., et al. (2007), Eddy-permitting Ocean circulation hindcasts of past decades, *CLIVAR Exchanges*, *42*(7), 8–10.
- Barron, C. N., and L. F. Smedstad (2002), Global river inflow within the Navy Coastal Ocean Model, in *Proceedings to Oceans 2002 MTS/IEEE Conference*, vol. 3, pp. 1472–1479, IEEE, Piscataway, N. J., doi:10.1109/OCEANS.2002.1191855.
- Bitz, C. M., and W. H. Lipscomb (1999), An energy-conserving thermodynamic model of sea ice, *J. Geophys. Res.*, *104*(C7), 15,669–15,677, doi:10.1029/1999JC900100.
- Brodeau, L., B. Barnier, T. Penduff, A. M. Treguier, and S. Gulev (2010), An ERA40-based atmospheric forcing for global ocean circulation models, *Ocean Modell.*, *31*(3–4), 88–104, doi:10.1016/j.ocemod.2009.10.005.
- Condron, A., P. Winsor, C. Hill, and D. Menemenlis (2009), Simulated response of the Arctic freshwater budget to extreme NAO wind forcing, *J. Clim.*, *22*, 2422–2437, doi:10.1175/2008JCLI2626.1.
- Curry, B., C. M. Lee, and B. Petrie (2011), Volume, freshwater, and heat fluxes through Davis Strait, 200405, *J. Phys. Oceanogr.*, *41*, 429–436, doi:10.1175/2010JPO4536.1.
- Dai, A., and K. E. Trenberth (2002), Estimates of freshwater discharge from continents: Latitudinal and seasonal variations, *J. Hydrometeorol.*, *3*, 660–687, doi:10.1175/1525-7541(2002)003<0660:EOFDFC>2.0.CO;2.
- Danabasoglu, G., S. Bates, B. P. Briegleb, S. R. Jayne, M. Jochum, W. G. Large, S. Peacock, and S. G. Yeager (2012), The CCSM4 ocean component, *J. Clim.*, *25*(5), 1361–1389, doi:10.1175/JCLI-D-11-00091.1.
- de Steur, L., E. Hansen, R. Gerdes, M. Karcher, E. Fahrbach, and J. Holfort (2009), Freshwater fluxes in the East Greenland Current: A decade of observations, *Geophys. Res. Lett.*, *36*, L23611, doi:10.1029/2009GL041278.
- Dodd, P. A., K. J. Heywood, M. P. Meredith, A. C. Naveira-Garabato, A. D. Marca, and K. K. Falkner (2009), The sources and fate of freshwater exported in the East Greenland Current, *Geophys. Res. Lett.*, *36*, L19608, doi:10.1029/2009GL039663.
- Döscher, R., K. Wyser, H. E. M. Meier, M. Qian, and R. Redler (2010), Quantifying Arctic contributions to climate predictability in a regional coupled ocean-ice-atmosphere model, *Clim. Dyn.*, *34*(7–8), 1157–1176, doi:10.1007/s00382-009-0567-y.
- Fanning, A. G., and A. J. Weaver (1996), An atmospheric energy-moisture model: Climatology, interpentadal climate change and coupling to an ocean general circulation model, *J. Geophys. Res.*, *101*(D10), 15,111–15,128, doi:10.1029/96JD01017.
- Fieg, K., R. Gerdes, E. Fahrbach, A. Beszczynska-Möller, and U. Schauer (2010), Simulation of oceanic volume transports through Fram Strait 1995–2005, *Ocean Dyn.*, *60*, 491–502, doi:10.1007/s10236-010-0263-9.
- Gent, P. R., et al. (2011), The Community Climate System Model version 4, *J. Clim.*, *24*(19), 4973–4991, doi:10.1175/2011JCLI4083.1.
- Gerdes, R., M. Karcher, and C. Köberle (2008), Simulating the long-term variability of liquid freshwater export from the Arctic Ocean, in *Arctic-Subarctic Ocean Fluxes*, edited by R. R. Dickson, J. Meincke, and P. Rhines, chap. 17, pp. 405–425, Springer, Dordrecht, Netherlands.
- Häkkinen, S. (1995), Simulated interannual variability of the Greenland Sea Deep Water formation and its connection to surface forcing, *J. Geophys. Res.*, *100*(C3), 4761–4770, doi:10.1029/94JC01900.
- Häkkinen, S., and G. L. Mellor (1992), Modeling the seasonal variability of a coupled Arctic ice-ocean system, *J. Geophys. Res.*, *97*(C12), 20,285–20,304, doi:10.1029/92JC02037.
- Häkkinen, S., and A. Proshutinsky (2004), Freshwater content variability in the Arctic Ocean, *J. Geophys. Res.*, *109*, C03051, doi:10.1029/2003JC001940.
- Herbaut, C., and M.-N. Houssais (2009), Response of the eastern North Atlantic subtropical gyre to the North Atlantic Oscillation, *Geophys. Res. Lett.*, *36*, L17607, doi:10.1029/2009GL039090.
- Hibler, W. D. (1979), A dynamic thermodynamic sea ice model, *J. Phys. Oceanogr.*, *9*, 815–846, doi:10.1175/1520-0485(1979)009<0815:ADTSIM>2.0.CO;2.
- Hibler, W. D. (1980), Modeling a variable thickness sea ice cover, *Mon. Weather Rev.*, *108*, 1943–1973, doi:10.1175/1520-0493(1980)108<1943:MAVTSI>2.0.CO;2.
- Holland, M. M., C. M. Bitz, M. Eby, and A. J. Weaver (2001), The role of ice-ocean interactions in the variability of the North Atlantic thermohaline circulation, *J. Clim.*, *14*(5), 656–675, doi:10.1175/1520-0442(2001)014<0656:TROIOL>2.0.CO;2.
- Holland, M. M., J. Finnis, A. P. Barrett, and M. C. Serreze (2007), Projected changes in Arctic Ocean freshwater budgets, *J. Geophys. Res.*, *112*, G04S55, doi:10.1029/2006JG000354.
- Holloway, G., et al. (2007), Water properties and circulation in Arctic Ocean models, *J. Geophys. Res.*, *112*, C04S03, doi:10.1029/2006JC003642.
- Houssais, M.-N., and C. Herbaut (2011), Atmospheric forcing on the Canadian Arctic Archipelago freshwater outflow and implications for the Labrador Sea variability, *J. Geophys. Res.*, *116*, C00D02, doi:10.1029/2010JC006323.
- Hunke, E. C., and J. K. Dukowicz (1997), An elastic-viscous-plastic model for sea ice dynamics, *J. Phys. Oceanogr.*, *27*(9), 1849–1867, doi:10.1175/1520-0485(1997)027<1849:AEVPMF>2.0.CO;2.
- Hunke, E. C., and W. H. Lipscomb (2008), CICE: the Los Alamos Sea Ice Model. Documentation and Software User’s Manual. Version 4.1, *Tech. Rep. LA-CC-06-012*, Los Alamos Natl. Lab., Los Alamos, N. M.
- Jahn, A., B. Tremblay, L. A. Mysak, and R. Newton (2010a), Effect of the large-scale atmospheric circulation on the Arctic Ocean freshwater and heat exchange, *Clim. Dyn.*, *34*(2–3), 201–222, doi:10.1007/s00382-009-0558-z.
- Jahn, A., L. B. Tremblay, R. Newton, M. M. Holland, L. A. Mysak, and I. A. Dmitrenko (2010b), A tracer study of the Arctic Ocean’s liquid freshwater export variability, *J. Geophys. Res.*, *115*, C07015, doi:10.1029/2009JC005873.
- Jahn, A., et al. (2012), Late 20th century simulation of Arctic sea ice and ocean properties in the CCSM4, *J. Clim.*, *25*(5), 1431–1452, doi:10.1175/JCLI-D-11-00201.1.
- Kalnay, E., et al. (1996), The NCEP/NCAR 40-year reanalysis project, *Bull. Am. Meteorol. Soc.*, *77*(3), 437–471, doi:10.1175/1520-0477(1996)077<0437:TNYRP>2.0.CO;2.
- Karcher, M., R. Gerdes, F. Kauker, C. Köberle, and I. Yashayaev (2005), Arctic Ocean change heralds North Atlantic freshening, *Geophys. Res. Lett.*, *32*, L21606, doi:10.1029/2005GL023861.
- Karcher, M., F. Kauker, R. Gerdes, E. Hunke, and J. Zhang (2007), On the dynamics of Atlantic Water circulation in the Arctic Ocean, *J. Geophys. Res.*, *112*, C04S02, doi:10.1029/2006JC003630.
- Karcher, M., A. Beszczynska-Möller, F. Kauker, R. Gerdes, S. Heyen, B. Rudels, and U. Schauer (2011), Arctic Ocean warming and its consequences for the Denmark Strait overflow, *J. Geophys. Res.*, *116*, C02037, doi:10.1029/2010JC006265.
- Killworth, P. D., D. Stainforth, D. J. Webb, and S. M. Paterson (1991), The development of a freesurface Bryan-Cox-Semtner ocean model, *J. Phys. Oceanogr.*, *21*(9), 1333–1348, doi:10.1175/1520-0485(1991)021<1333:TDOAFS>2.0.CO;2.
- Köberle, C., and R. Gerdes (2003), Mechanisms determining the variability of Arctic sea ice conditions and export, *J. Clim.*, *16*(17), 2843–2858, doi:10.1175/1520-0442(2003)016<2843:MDTVOA>2.0.CO;2.

- Köberle, C., and R. Gerdes (2007), Simulated variability of the Arctic Ocean freshwater balance 1948–2001, *J. Phys. Oceanogr.*, 37(6), 1628–1644, doi:10.1175/JPO3063.1.
- Kwok, R. (2005), Variability of Nares Strait ice flux, *Geophys. Res. Lett.*, 32, L24502, doi:10.1029/2005GL024768.
- Kwok, R., and D. A. Rothrock (1999), Variability of Fram Strait ice flux and North Atlantic Oscillation, *J. Geophys. Res.*, 104(C3), 5177–5190, doi:10.1029/1998JC900103.
- Kwok, R., G. F. Cunningham, and S. S. Pang (2004), Fram Strait sea ice outflow, *J. Geophys. Res.*, 109, C01009, doi:10.1029/2003JC001785.
- Kwok, R., W. Maslowski, and S. W. Laxon (2005), On large outflows of Arctic sea ice into Barents Sea, *Geophys. Res. Lett.*, 32, L22503, doi:10.1029/2005GL024485.
- Kwok, R., G. F. Cunningham, M. Wensnahan, I. Rigor, H. J. Zwally, and D. Yi (2009), Thinning and volume loss of the Arctic Ocean sea ice cover: 2003–2008, *J. Geophys. Res.*, 114, C07005, doi:10.1029/2009JC005312.
- Lammers, R. B., A. I. Shiklomanov, C. J. Vörösmarty, B. M. Fekete, and B. J. Peterson (2001), Assessment of contemporary Arctic river runoff based on observational discharge records, *J. Geophys. Res.*, 106(D4), 3321–3334, doi:10.1029/2000JD900444.
- Large, W. G., and S. G. Yeager (2004), Diurnal to decadal global forcing for ocean and sea-ice models: The data sets and flux climatologies, *Tech. Rep. TN-460+str*, Natl. Cent. for Atmos. Res., Boulder, Colo.
- Large, W. G., and S. G. Yeager (2009), The global climatology of an inter-annually varying air–sea flux data set, *Clim. Dyn.*, 33(2–3), 341–364, doi:10.1007/s00382-008-0441-3.
- Levitus, S. (1982), Climatological Atlas of the World Ocean, *Prof. Pap. 13 (NTISPB83-184093)*, NOAA/ERL GFDL, Princeton, N. J.
- Lipscomb, W. H. (2001), Remapping the thickness distribution in sea ice models, *J. Geophys. Res.*, 106(C7), 13,989–14,000, doi:10.1029/2000JC000518.
- Lique, C., A. M. Treguier, M. Scheinert, and T. Penduff (2009), A model based study of ice and freshwater transport variability along both sides of Greenland, *Clim. Dyn.*, 33(5), 685–705, doi:10.1007/s00382-008-0510-7.
- Lique, C., A. M. Treguier, B. Blanke, and N. Grima (2010), On the origins of water masses exported along both sides of Greenland: A Lagrangian Model Analysis, *J. Geophys. Res.*, 115, C05019, doi:10.1029/2009JC005316.
- Locarnini, R. A., A. V. Mishonov, J. I. Antonov, T. P. Boyer, and H. E. Garcia (2006), *World Ocean Atlas 2005*, vol. 1, *Temperature*, NOAA Atlas NESDIS 61, edited by S. Levitus, 182 pp., U.S. Govt. Print. Off., Washington, D. C.
- Lohmann, G., and R. Gerdes (1998), Sea ice effects on the sensitivity of the thermohaline circulation, *J. Clim.*, 11(11), 2789–2803, doi:10.1175/1520-0442(1998)011<2789:SIEOTS>2.0.CO;2.
- Losch, M., D. Menemenlis, P. Heimbach, J. Campin, and C. Hill (2010), On the formulation of sea-ice models. Part 1: Effects of different solver implementations and parameterizations, *Ocean Modell.*, 33(1–2), 129–144, doi:10.1016/j.oceomod.2009.12.008.
- Madec, G. (2008), NEMO Ocean engine, *Note du pôle modélisation 27*, IPSL, Paris.
- Marshall, J., A. Adcroft, C. Hill, L. Perelman, and C. Heisey (1997), A finite-volume, incompressible Navier-Stokes model for studies of the ocean on parallel computers, *J. Geophys. Res.*, 102(C3), 5753–5766, doi:10.1029/96JC02775.
- Mårtensson, S., H. E. M. Meier, P. Pemberton, and J. Haapala (2012), Ridged sea ice characteristics in the Arctic from a coupled multicategory sea ice model, *J. Geophys. Res.*, 117, C00D15, doi:10.1029/2010JC006936.
- Maykut, G. A., and N. Untersteiner (1971), Some results from a time-dependent thermodynamic model of sea ice, *J. Geophys. Res.*, 76(6), 1550–1575, doi:10.1029/JC076i006p01550.
- McPhee, M. G., A. Proshutinsky, J. H. Morison, M. Steele, and M. B. Alkire (2009), Rapid change in freshwater content of the Arctic Ocean, *Geophys. Res. Lett.*, 36, L10602, doi:10.1029/2009GL037525.
- Meier, H. E. M., R. Döscher, and T. Faxén (2003), A multiprocessor coupled ice-ocean model for the Baltic Sea: Application to salt inflow, *J. Geophys. Res.*, 108(C8), 3273, doi:10.1029/2000JC000521.
- Melling, H., T. A. Agnew, K. K. Falkner, D. A. Greenberg, C. M. Lee, A. Münchow, B. Petrie, S. J. Prinsenber, R. M. Samelson, and R. A. Woodgate (2008), Fresh-water fluxes via Pacific and Arctic outflows across the Canadian polar shelf, in *Arctic-Subarctic Ocean Fluxes*, edited by R. R. Dickson, J. Meincke, and P. Rhines, chap. 9, pp. 193–247, Springer, Dordrecht, Netherlands.
- Menemenlis, D., I. Fukumori, and T. Lee (2005), Using Green’s functions to calibrate an ocean general circulation model, *Mon. Weather Rev.*, 133, 1224–1240, doi:10.1175/MWR2912.1.
- Münchow, A., and H. Melling (2008), Ocean current observations from Nares Strait to the west of Greenland: Interannual to tidal variability and forcing, *J. Mar. Res.*, 66, 801–833.
- Münchow, A., H. Melling, and K. K. Falkner (2006), An observational estimate of volume and freshwater flux leaving the Arctic Ocean through Nares Strait, *J. Phys. Oceanogr.*, 36(11), 2025–2041, doi:10.1175/JPO2962.1.
- Nguyen, A., D. Menemenlis, and R. Kwok (2009), Improved modeling of the Arctic halocline with a subgrid-scale brine rejection parameterization, *J. Geophys. Res.*, 114, C11014, doi:10.1029/2008JC005121.
- Nguyen, A., D. Menemenlis, and R. Kwok (2011), Arctic ice-ocean simulation with optimized model parameters: Approach and assessment, *J. Geophys. Res.*, 116, C04025, doi:10.1029/2010JC006573.
- Onogi, K., et al. (2007), The JRA-25 reanalysis, *J. Meteorol. Soc. Jpn.*, 85(3), 369–432, doi:10.2151/jmsj.85.369.
- Pacanowski, R. (1995), MOM 2 documentation, user’s guide, and reference manual, GFDL Ocean Group technical report, NOAA, Princeton, N. J.
- Pacanowski, R. C., and A. Gnanadesikan (1998), Transient response in a z-level ocean model that resolves topography with partial cells, *Mon. Weather Rev.*, 126(12), 3248–3270, doi:10.1175/1520-0493(1998)126<3248:TRIAZL>2.0.CO;2.
- Penduff, T., J. Le Sommer, B. Barnier, A.-M. Treguier, J.-M. Molines, and G. Madec (2007), Influence of numerical schemes on current-topography interactions in 1/4° global ocean simulations, *Ocean Sci.*, 3, 509–524.
- Prange, M. (2003), Einfluss arktischer Süßwasserquellen auf die Zirkulation im Nordmeer und im Nordatlantik in einem prognostischen Ozean-Meereis-Modell, *Polar Mar. Res.*, 46(8), 220 pp.
- Prinsenber, S. J., and J. Hamilton (2005), Monitoring the volume, freshwater and heat fluxes passing through Lancaster Sound in the Canadian Arctic Archipelago, *Atmos. Ocean*, 43(1), 1–22.
- Prinsenber, S., J. Hamilton, I. Peterson, and R. Pettipas (2009), Observing and interpreting the seasonal variability of the oceanographic fluxes passing through Lancaster Sound of the Canadian Arctic Archipelago, in *Influence of Climate Change on the Changing Arctic and Sub-Arctic Conditions*, NATO Sci. Peace Secur. Ser. C: Environmental Security, edited by J. C. J. Nihoul and A. G. Kostianoy, pp. 125–143, Springer, Dordrecht, Netherlands.
- Proshutinsky, A., R. Krishfield, M.-L. Timmermans, J. Toole, E. Carmack, F. McLaughlin, W. J. Williams, S. Zimmermann, M. Itoh, and K. Shimada (2009), Beaufort Gyre freshwater reservoir: State and variability from observations, *J. Geophys. Res.*, 114, C00A10, doi:10.1029/2008JC005104.
- Proshutinsky, A., et al. (2011), Recent advances in Arctic Ocean studies employing models from the Arctic Ocean Model Intercomparison Project, *Oceanography*, 24(3), 102–113, doi:10.5670/oceanog.2011.61.
- Rabe, B., A. Münchow, H. L. Johnson, and H. Melling (2010), Nares Strait hydrography and salinity field from a 3-year moored array, *J. Geophys. Res.*, 115, C07010, doi:10.1029/2009JC005966.
- Rabe, B., M. Karcher, U. Schauer, J. M. Toole, R. A. Krishfield, S. Pisarevc, F. Kauker, R. Gerdes, and T. Kikuchi (2011), An assessment of Arctic Ocean freshwater content changes from the 1990s to the 2006–2008 period, *Deep Sea Res.*, 58(5), 173–185, doi:10.1016/j.dsr.2010.12.002.
- Rawlins, M. A., et al. (2010), Analysis of the Arctic system for freshwater cycle intensification: Observations and expectations, *J. Clim.*, 23, 5715–5737, doi:10.1175/2010JCLI3421.1.
- Rennermalm, A. K., E. F. Wood, S. J. Déry, A. J. Weaver, and M. Eby (2006), Sensitivity of the thermohaline circulation to Arctic Ocean runoff, *Geophys. Res. Lett.*, 33, L12703, doi:10.1029/2006GL026124.
- Rennermalm, A. K., E. F. Wood, A. J. Weaver, M. Eby, and S. J. Déry (2007), Relative sensitivity of the Atlantic Meridional Overturning Circulation to river discharge into Hudson Bay and the Arctic Ocean, *J. Geophys. Res.*, 112, G04S48, doi:10.1029/2006JG000330.
- Rigor, I. G., R. L. Colony, and S. Martin (2000), Variations in surface air temperature observations in the Arctic, 1979–97, *J. Clim.*, 13(5), 896–914, doi:10.1175/1520-0442(2000)013<0896:VISATO>2.0.CO;2.
- Romanov, I. P. (2004), Morphometric characteristics of ice and snow in the Arctic Basin: aircraft landing observations from the Former Soviet Union, digital media, Natl. Snow and Ice Data Cent., Boulder, Colo. [Available at <http://nsidc.org/data/g02140.html>]
- Schweiger, A., R. Lindsay, J. Zhang, M. Steele, H. Stern, and R. Kwok (2011), Uncertainty in modeled Arctic sea ice volume, *J. Geophys. Res.*, 116, C00D06, doi:10.1029/2011JC007084.
- Semtner, A. (1976), A model for the thermodynamic growth of sea ice in numerical investigations of climate, *J. Phys. Oceanogr.*, 6, 379–389.
- Serreze, M. C., A. P. Barrett, A. G. Slater, R. A. Woodgate, K. Aagaard, R. B. Lammers, M. Steele, R. Moritz, M. Meredith, and C. M. Lee (2006), The large-scale freshwater cycle of the Arctic, *J. Geophys. Res.*, 111, C11010, doi:10.1029/2005JC003424.

- Smith, R., et al. (2010), The Parallel Ocean Program (POP) reference manual, *Tech. Rep. LAUR-10-01853*, Los Alamos Natl. Lab., Los Alamos, N. M.
- Smith, R. D., J. K. Dukowicz, and R. C. Malone (1992), Parallel ocean general circulation modeling, *Phys. D*, *60*(1–4), 38–61, doi:10.1016/0167-2789(92)90225-C.
- Steele, M., R. Morley, and W. Ermold (2001), PHC: A global ocean hydrography with a high-quality Arctic Ocean, *J. Clim.*, *14*(9), 2079–2087, doi:10.1175/1520-0442(2001)014<2079:PAGOHW>2.0.CO;2.
- Stevens, D. (1991), The open boundary condition in the United Kingdom fine resolution Antarctic model, *J. Phys. Oceanogr.*, *21*, 1494–1499, doi:10.1175/1520-0485(1991)021<1494:TOBCIT>2.0.CO;2.
- Thorndike, A. S., D. S. Rothrock, G. A. Maykut, and R. Colony (1975), Thickness distribution of sea ice, *J. Geophys. Res.*, *80*(C33), 4501–4513, doi:10.1029/JC080i033p04501.
- Timmermann, R., H. Goosse, G. Madec, T. Fichefet, C. Etche, and V. Duliere (2005), On the representation of high latitude processes in the ORCA-LIM global coupled sea ice-ocean model, *Ocean Modell.*, *8*(1–2), 175–201, doi:10.1016/j.ocemod.2003.12.009.
- Tsubouchi, T., S. Bacon, A. C. Naveira Garabato, S. W. L. Y. Aksenov, E. Fahrbach, A. Beszczynska-Möller, E. Hansen, C. M. Lee, and R. Ingvaldsen (2012), The Arctic Ocean in summer: A quasi-synoptic inverse estimate of boundary fluxes and water mass transformation, *J. Geophys. Res.*, *117*, C01024, doi:10.1029/2011JC007174.
- Uppala, S. M., et al. (2005), The ERA-40 re-analysis, *Q. J. R. Meteorol. Soc.*, *131*(612), 2961–3012, doi:10.1256/qj.04.176.
- Vinje, T., N. Nordlund, and Å. Kvambekk (1998), Monitoring ice thickness in Fram Strait, *J. Geophys. Res.*, *103*(C5), 10,437–10,449, doi:10.1029/97JC03360.
- Weaver, A. J., J. Marotzke, P. F. Cummins, and E. Sarachik (1993), Stability and variability of the thermohaline circulation, *J. Phys. Oceanogr.*, *23*(1), 39–60, doi:10.1175/1520-0485(1993)023<0039:SAVOTT>2.0.CO;2.
- Weaver, A. J., et al. (2001), The UVic Earth System Climate Model: Model description, climatology and application to past, present and future climates, *Atmos. Ocean*, *39*(4), 361–428.
- Woodgate, R. A., and K. Aagaard (2005), Revising the Bering Strait freshwater flux into the Arctic Ocean, *Geophys. Res. Lett.*, *32*, L02602, doi:10.1029/2004GL021747.
- Woodgate, R. A., K. Aagaard, and T. J. Weingartner (2005), Monthly temperature, salinity, and transport variability of the Bering Strait through flow, *Geophys. Res. Lett.*, *32*, L04601, doi:10.1029/2004GL021880.
- Zhang, J., and W. D. Hibler (1997), On an efficient numerical method for modeling sea ice dynamics, *J. Geophys. Res.*, *102*(C4), 8691–8702, doi:10.1029/96JC03744.
- Zhang, J., and D. Rothrock (2001), A thickness and enthalpy distribution sea-ice model, *J. Phys. Oceanogr.*, *31*, 2986–3001, doi:10.1175/1520-0485(2001)031<2986:ATAEDS>2.0.CO;2.
- Zhang, J., and D. A. Rothrock (2003), Modeling global sea ice with a thickness and enthalpy distribution model in generalized curvilinear coordinates, *Mon. Weather Rev.*, *131*(5), 845–861, doi:10.1175/1520-0493(2003)131<0845:MGSIWA>2.0.CO;2.
- Zhang, J., and D. A. Rothrock (2005), The effect of sea-ice rheology in numerical investigations of climate, *J. Geophys. Res.*, *110*, C08014, doi:10.1029/2004JC002599.
- Zhang, X., M. Ikeda, and J. Walsh (2003), Arctic sea ice and freshwater changes driven by the atmospheric leading mode in a coupled sea ice-ocean model, *J. Clim.*, *16*(13), 2159–2177, doi:10.1175/2758.1.